Magic numbers for shells of electrons and shells of atoms in binary clusters

S. Neukermans, E. Janssens, R. E. Silverans, P. Lievens

Laboratorium voor Vaste-Stoffysica en Magnetisme, Katholieke Universiteit Leuven,

Celestijnenlaan 200D, B-3001 Leuven, Belgium

14 October 2006

1. Introduction

The human interest in cluster physics may be a few hundred or thousand years older than what we generally assume. At least, several of the highly symmetric structures often encoutered in clusters already intrigued human beings as early as the New Stone Age (Neolithicum) [1]. Hundreds of carved stones with lines corresponding to the edges of regular polyhedra were found in Scotland and believed to date back to around 2000 B.C.[2]. The icosahedron and dodecahedron were known to the ancient Greeks and described by Plato as two of the five Platonic solids, besides the tetrahedron, cube, and octahedron. Dating back to the Roman time (second to fourth century), dozens of hollow bronze dodecahedra (Figure 1) have been found in Austria, Belgium, France, Germany, Great Britain, Hungary, Luxembourg, the Netherlands, and Switzerland. Artmann also reports a Roman icosahedron, which, misclassified as a dodecahedron, was stored in a museum's basement for fourty years before it got recognized as an icosahedron [3]. But, as is the case for the carved stones found in Scotland, their function remains mysterious.

Even if it seems quite unlikely that people in ancient times had atomic clusters in mind, the possible existence of highly symmetric species constitutes a major issue in current atomic cluster physics. Although governed by the same fundamental laws, the physics of clusters is very different from their analogues on a macroscopic scale. Nanometer-sized pieces of matter show magnetic, optical, chemical, catalytic… properties different and often superior to their bulk counterparts. In this respect, in particular clusters composed of two types of atoms are considered to be very attractive study objects as one can flexibly tune the unique physico-

chemical properties of clusters by controlling their composition. After all, binary clusters composed of elements with different valences allow to vary the total number of electrons independently of the number of constituent atoms.

Playing around with the number and type of building blocks (nuclei and electrons) in atomic clusters was not arbitrarily invented merely to extend the range of cluster systems to be investigated. Pioneering mass spectrometric observations immediately revealed the influence of the number of atoms or the number of electrons, depending on the type of its constituent atoms, on the stability of clusters. The physical origin of the importance of the exact number of atoms or electrons, compared to bulk matter, relates to the large surface to volume ratio on one hand, and to the finite spacing between electronic energy levels or *energy quantization* in small clusters on the other hand.

In clusters composed of rare gas atoms the interatomic interactions are weak and isotropic. These aggregates are observed to form close-packed structures as was discovered in 1981 in a mass spectrum of xenon clusters by Echt and coworkers, which showed pronounced peaks or steps in abundances for clusters containing a 'magic number' of 13, 55, 147… atoms [4]. The intervals between these numbers correspond to the completion of an additional layer of xenon atoms, consisting of 20 regular triangular faces arranged concentrically around the central atom forming the symmetric icosahedral structures described by Mackay [5]. As such, the origin of these magic numbers is related to the geometric packing, or to *shells of atoms* in the clusters.

On the other hand, clusters composed of alkali metal atoms feature metallic bonds provided by the itinerant valence electrons of the constituent atoms. The identification of magic numbers (2, 8, 20, 40, 58…) and their interpretation in terms of an electronic shell structure in small clusters of sodium in 1984 by Knight and co-workers [6], in one stroke inspired numerous research groups to embark on the line of cluster research.

Where the packing in rare gases is interesting but more of a 'fait-divers', the study of metals is much more central to the subject of condensed matter physics and chemistry in general. The shell structure identified in alkali metal clusters has nothing to do with the packing of atoms. It is attributed to a delocalization behavior of valence electrons of the constituent atoms. Each conduction electron is delocalized over the entire cluster volume and occupies a one-particle

state in a centro-symmetric potential well. Clusters in which the number of delocalized electrons corresponds to the number of electrons required to fill an electronic shell are more stable and as such observed more abundantly. This is illustrated in Figure 2 (left) for the case of pure gold cluster cations after photofragmentation. In the mass spectrum steps in abundance are observed after cluster sizes containing 2, 8, 18, 20, 34… valence electrons. These numbers correspond to electronic shell filling numbers in the sequence of spherical shells 1*s*/1*p*/1*d*/2*s*/1*f*/…. Contrary to simple (alkali, noble) metal clusters, in the case of transition metal clusters such as titanium (Figure 1.2 right) enhanced stabilities are observed for cluster sizes 7, 13, 15, 19… corresponding to symmetric geometric structures.

Ever since, the quest for both geometrically and electronically closed shell, and consequently very stable *magic* species is a leading thread in current cluster research. Highly symmetric clusters, presenting special structural, as well as electronic and thermodynamic stability, with tailored physical and chemical properties look very attractive as building blocks for nanostructured materials. And as mentioned above, aside from highly symmetric systems like C_{60} [7], binary or doped clusters are well suited for this purpose, since they inherently offer the possibility of altering cluster properties nearly at will by varying the number of atoms independently of the number of itinerant electrons.

The study of (binary) clusters is interdisciplinary by definition. While in inorganic chemistry and solid state chemistry a traditional quest has been to understand how materials are built up by combining different atoms, similarly, condensed matter physics has been aiming to understand the fundamentals of bulk properties by investigating small scale precursors. Evidently, the complexity of this interdisciplinary field can not be covered in a short review. Here, we will restrict the discussion to sets of mixed clusters where the interpretation of their properties strongly relies on shell structure descriptions, both shells of electrons and shells of atoms. This chapter reviews recent studies of small binary clusters, with less than 100 atoms per clusters. Because of these small sizes, many of the species can be considered as molecules, implying the use of molecular language when describing their structure. In this review we will combine this with terminology borrowed from condensed matter physics.

Two introductory sections give a concise description of how binary clusters are produced, and a summary of relevant cluster models, respectively. In the bulk of the fourth section, three

types of binary cluster systems will be reviewed: electronegatively doped main group metals, transition metal doped noble metals, and metal doped semi-metal clusters. In all three cases special attention will be given to binary systems in which the interplay between electronic shell closing and specific geometries gives rise to pronounced or exceptional physico-chemical (stability, reactivity, magnetic…) properties.

2. Production

A general overview of the different types of single element cluster sources is given in ref. 8. Several cluster sources for producing binary clusters in a controlled way have been reported. Nearly all types of single element cluster sources can be used to produce binary clusters, which contain one element that is available as a gas (component), through the addition of (small amounts of) that reactant gas to the inert carrier gas of the source. The cluster composition can be tuned by controlling the partial pressure of the reactant gas. Typical examples of dopant gasses added to the carrier gas are O_2, Cl_2, H_2O, …[9] Although this technique is important and widely applied in particular for the study of metal cluster oxides, the variety of binary systems that can be produced is rather limited.

Bimetallic clusters have been produced by a single mixed-cartridge [10,11] or dual cartridge [9] hot oven source. In the former the relative abundance of the constituent elements can be adjusted by changing the mixing ratio in the cartridge, but is limited to a single evaporation temperature for both elements and thus to fixed relative vapor pressures. The latter improves this concept by including separate temperature control for the two metals, allowing a larger range of mixing ratios. Applications of hot oven sources or thermal cluster sources are restricted to low boiling point metals and usually produce relatively hot clusters. The first use of both a single mixed cartridge [10] and dual cartridge [9] oven source was reported by T.P. Martin to produce arsenic sulfide clusters and cesium sulfide clusters, respectively.

Laser vaporization sources [12] are an alternative to hot oven sources for the production of bimetallic clusters. Although the thermodynamical properties of this kind of source are not as well described, it allows cluster production of a greater variety of materials and produces colder clusters ($T \leq 300$ K). Binary metallic clusters have been produced by a variety of laser

vaporization sources: single target sources using binary alloy targets [13,14], pressed mixed powders [15], or coated rods [16], and dual-rod target sources using a split vaporization laser beam [17] or two vaporization lasers [18,19]. The latter type, using two separate lasers for two separate targets, originally developed by Kaya and coworkers, has demonstrated to be the most versatile technique [20,21,22]. In Figure 3 a schematic overview is given of two types of dual-target dual-laser vaporization sources of Kaya [18] and Lievens [19], respectively. The use of two independent lasers allows varying energy and vaporization timing independently. The amount of introduced helium can be controlled through the gas valve. Cluster formation in a laser vaporization source is strongly dependent on the amount of three body collisions and the particle temperature, which is determined by collisions with the carrier gas atoms. This implies that the densities of the constituent elements and the carrier gas in the formation chamber are governing the aggregation process. The composition of the bimetallic clusters can be controlled by varying the partial pressures of the two metal vapors and the helium gas. The metal vapor pressures depend on the vaporization laser energies and the time delays of the laser pulses with respect to the gas pulse. Furthermore, the cluster formation is influenced by the source geometry, in particular the volume of the formation chamber and the shape of the nozzle.

To our knowledge, the use of other types of cluster sources for the production of bimetallic species is very rare. An example is the production of Au_nAg_m clusters from a sputtering source with silver-gold alloy targets [23].

3. Modeling

Binary clusters not only impose an additional degree of complexity on experiments but also on theoretical models. In nearly all first-principles calculational approaches to the many-particle problem of a cluster, replacing one or more atoms (X) in a homoatomic cluster (X_n) by one or more atoms of a different element (Y) drastically increases the number of possible structural isomers that have to be probed for optimization. Pioneering *ab initio* quantum chemical studies on different binary cluster systems already started in the late eighties [24,25,26,27,28]. Although computational resources are rapidly evolving, quantum

chemical computational studies of binary cluster systems still remain restricted to the smaller sizes (typically less than about 15 to 20 atoms) or high symmetries. Larger systems have been studied using molecular dynamics [29,30] .

Luckily, several (size-dependent) properties of simple metal (alkali, noble) clusters are not drastically influenced by the details of the ionic structure. In a *jellium* model a significant simplification to the quantum mechanical many particle problem is achieved, at the expense of computational accuracy, by introducing a constant potential replacing the effect of the ions and core electrons in the cluster. Only the many-body problem of the valence electrons confined by the interaction with this homogeneous distribution of positive charges is treated self-consistently with density functional theory [31]. *Phenomenological shell models*, inspired by the nuclear shell model, simplify the computational problem of a cluster even further and only consider the possible states of a single electron confined in a potential well of a given shape [8]. Nevertheless, the shell model is able to explain qualitative electronic shell effects in size-dependent properties of simple (alkali, noble) metal clusters, where the valence electrons of the constituent atoms can be considered itinerant. However, it is not a priori clear if this behavior can be extrapolated to heterogeneous clusters composed of two different (simple) metals. The different electron density, electron affinity, and ionization energy of the dopant atom perturbs the effective potential experienced by the valence electrons. The electronic energy level sequence and the electron delocalization behavior also are affected by this modified potential.

If the valence electrons are itinerant, completely occupied electron states are responsible for enhanced stability and abundance maxima are expected to occur at electron numbers 2, 8, 20, 34, 40… for spherical-like shapes. This should be the case irrespective of the number of cores contributing to the effective potential and in spite of the heterogeneous ionic structure. Experimental studies on doped alkaline [32,33,34,35,36,37,38], aluminum [39,40], and coinage [41,42,43] metal clusters indeed showed that the free electron picture remains valid, at least to a certain extent. More stable clusters correspond to systems where the total amount of valence electrons equals one of the known spherical magic numbers.

However, a number of stable heterogeneous clusters were found, which correspond to electron numbers that are not observed for single element clusters. Evidence for a magic

number corresponding to 10 electrons was found in clusters doped with electronegative elements, such as K_8Zn, Na_9Au, Na_6Pb, K_8Mg, and Na_8Zn [33,36,37,38], while 18 is a pronounced magic number in species doped with electropositive elements, such as $Au_{18}Cu^+$, $Au_{16}Al^+$, and $Au_{16}In^+$ [41,42]. These novel magic numbers were related to dopant induced changes in the energy level sequence. The standard *jellium model* is inadequate to explain these changes, since it assumes a uniformly charged background. A *two-step spherical jellium model* was introduced to deal with this shortcoming. Host and impurity atoms are both characterized by a uniform but different positively charged background [44,45,46]. Similarly, a *modified phenomenological* (Wood-Saxon) potential was used to account for the 'new' magic numbers observed in doped alkali cluster systems [36]. The latter is illustrated in Figure 4. In both approaches two situations can be distinguished [47], as illustrated schematically in Figure 5.

(i) If the central heteroatom is more electronegative than the host atoms, the effective potential is more attractive at the center of the cluster. Orbitals that have (most of) their density in the center (i.e., *s*, and to a lesser extent *p* levels) will energetically be favored, while orbitals that have several nodal planes crossing the origin (*d* and *f* levels) remain relatively unaffected. The deeper the depression, the more the n*s* states are pulled down. A small depression results in a shift of the energy levels and fades electronic shell closings for 18 and 34 electrons. A stronger depression results in 1*d*/2*s* and 1*f*/2*p* level inversions and the new magic numbers 10 and 26, while the 18 and 34 electron shell closures disappear. The level sequence becomes 1*s*/1*p*/2*s*/1*d*/2*p*/1*f*/… with corresponding magic numbers 2, 8, 10, 20, 26, 40… (see Figure 5(b)).

(ii) If the central heteroatom is less electronegative than the host atoms, it causes a hump in the center of the potential. This leads to an upward shift of the ns levels relative to the levels with non-zero angular momentum. Regardless of the exact shape of the potential this again will cause level shifts, e.g., enlarge the gap between the 1*d* and 2*s* levels, and decrease the spacing between the 2*s* and 1*f* levels. The magic number 20 disappears in favor of the magic number 18, resulting in a 1*s*/1*p*/1*d*/2*s*/1*f*/2*p*/… level sequence with magic numbers 2, 8, 18, 34, 40… (see Figure 5(c)).

It should be noted that the modified jellium or phenomenological models only hold for (centro-symmetrically) singly doped species or segregated binary clusters, since a spherical symmetry is assumed and both models naively incorporate the ionic structure. For clusters with a reduced symmetry, for example if the hetero-atom is in an off-center position, one may no longer be able to assign electron shells and energy levels using a simple phenomenological potential. Also in multiply-doped species (*alloy* clusters) or doped metal clusters composed of atoms with a large difference in electronegativity the manifestation of electronic shell effects in their physico-chemical properties can be strongly suppressed because of the formation of covalent/directional and/or ionic bonds.

Size–dependent features in the properties of certain types of clusters cannot be explained using simplifying electronic shell models. The magic behavior in their properties depends more on the atomic packing or the optimization of *d-d* interactions and is governed by symmetric geometric structures, often termed *shells of atoms* [48]. This is, in general, the case for larger clusters of nearly all materials since the band of electronic states broadens and the HOMO-LUMO gap, which is a measure for the electronic shell closing effect, becomes small. However for certain clusters atomic shells or close-packed structures also are important in the small size range. Transition metal clusters, due to the presence of partially occupied *d* states, feature magic numbers that correspond to symmetric close-packed structures, for example 7 (bicapped pentagon or half icosahedron), 13 (icosahedron), 15 (BCC-unit), 19 (double icosahedron), etc. But also clusters of covalently bound non-metals usually have more open geometries that satisfy the specific highly directional bonding requirements of these elements [49]. Carbon species may adopt geometries as diverse as chains, rings, graphene sheets, fullerenes and nanotubes. Silicon and germanium clusters, up to $n \approx 25 - 35$, form prolate structures that are built by stacking exceptionally stable Si_9 and Ge_9 tricapped trigonal prism units [50,51], and rearrange to more spherical morphologies for larger sizes.

Important is the fact that the stability of several of these geometries can be further enhanced by proper doping. The stability of a 13-atom icosahedron can be enhanced by substituting the central atom by a suitable hetero atom. This arises due to the fact that the vertex-vertex bonds (a) are about 5 % longer than center-vertex bonds (R)

$$R = \frac{5^{1/4}}{2}\sqrt{\phi}a$$

where $\phi = \left(1+\sqrt{5}\right)/2 = 1{,}618...$ is the golden ratio or divine proportion. For example, symmetric Si_n and Ge_n cages are known to be stabilized by transition metal encapsulation. Hereby the open d-band of the transition metal dopant is crucial to host the dangling bond electrons of the surrounding Si_n or Ge_n cages [52,53].

4. A selection of different systems

4.1 Electronegatively doped group I, II, and III metal clusters

Metallic clusters doped with electronegative elements ((C), O, S, F, Cl, I…) probably are the oldest type of binary cluster systems that have been investigated. An important reason therefore is experimental, since no dual cluster source is required because the dopants can be added in gaseous form to the carrier gas of the source. Depicting a single pioneering study on metal clusters doped with electronegative elements is very difficult. Nevertheless, the identification of Li_3O, by Wu and coworkers [54] in 1979, as a very stable molecule in a mass spectrometric analysis of the vapor from Knudsen effusion of solid lithium oxide, can be regarded as an important step in the onset of binary metal cluster physics and chemistry. Despite the fact that the normal octet rule in traditional chemical bonding is violated, its dissociation energy towards the corresponding octet molecule Li_2O was found to be very high (2.45 ± 0.50 eV) [54].

About four years later, the origin of the unusual stability observed for Li_3O, was revealed by Schleyer and coworkers, who computationally investigated a large number of stable M_nX molecules, having polycoordinated central atoms (X), which suggest violation of the octet rule [26]. In these species, excess electrons (beyond the usual octet) populate orbitals with a highly delocalized character. Such orbitals, usually the highest occupied molecular orbital (HOMO), are antibonding with respect to M − X, but bonding with respect to M − M.

Species with this behavior have been termed hypermetallated, and numerous examples exist. They all exhibit an exceptional stability although formally the octet rule in the chemical

bonding is violated. For example, also Li_4O, Li_5O, Li_5C, and Li_6C are found to be thermodynamically stable towards all possible dissociation modes [26,27,55,56,57,58]. In Figure 6 a mass abundance spectrum of lithium-carbon clusters is shown featuring the exceptional stability of Li_6C [55,59] The energy level sheme and corresponding molecular orbitals show a 10 electron closed shell structure ($1s^2/1p^6/2s^2$) and the HOMO orbital that is antibonding with respect to Li – C but strongly Li – Li bonding. Many examples have been studied computationally [26,27,56,60,61] and identified experimentally [55,58,62,63,64]. In general, hypermetallic species (M_nX) consist of an electronegative main group element (X = O, C, N, B, F, Cl, S, P, Be…) surrounded by a shell of metal atoms (M = Li, Na, K, Mg, Al, In, Si…). Notice that Li_3O can be considered as a sort of *cluster precursor* since the classical chemical bonding in *normal* molecules (directional and fully saturated bonds) is violated. Instead, an excess electron in an orbital delocalized over the entire system provides extra bonding. This delocalized electronic bonding is a typical characteristic for metal clusters compared to regular molecules.

Along with the development of cluster sources also larger clusters composed of mixtures of electronegative and metal atoms could be studied. One particular example is a class of molecular clusters, the so-called Met-Cars (short for Metallo-Carbohedrenes), where for a number of mixed carbon and transition metal clusters specific stoichiometries and sizes with enhanced stability were discovered [65]. Another subset is formed by alkali metals with electronegative elements. In several cases such systems, e.g., Cs_nO_m, Li_nO_m, Li_nC, Na_nO_m, Li_nH_m, Na_nF_m [59,66,67,68,69,70,71], showed segregation between an ionically bound bulk-like crystallite and a metallic part with properties very similar to bare metal clusters. In the case of oxygen doped clusters, segregation or alloy formation strongly depends on the dopant concentration. In a threshold photoionization study of (monovalent) cesium oxide clusters, peculiarly high ionization energy values were found for $Cs_{z+2n}O_n$ species with z = 8, 18, 34, 58, 92…, sizes that correspond to magic numbers resulting from a simple spherical shell model [68]. Most probably, segregation occurs between an ionically bound $Cs_{2n}O_n$ unit and a shell of z surrounding Cs atoms, which leads to the unexpected spherically symmetric potential well in which z delocalized valence electrons are moving. In oxygen or carbon doped lithium clusters electronic shell closings could be identified in the size dependent pattern of

the ionization energies [59,66,67]. In a photofragmentation an evaporation study of metal rich lithium oxide clusters $Li_p^+(Li_2O)_n$ loss of metallicity was observed for increasing size (n) of the oxide component [72]. As illustrated in Figure 7, the results show vanishing of the odd-even alternation and the disappearance of an electronic shell closing. Another example is a unimolecular evaporation study of lithium rich $Li_nH_m^+$ cluster ions, which indicated a clear separation between a metallic Li_{n-m}^+ part and an insulating $(LiH)_m$ part [71].

The picture appears to be completely different in the case of divalent metal oxide clusters, e.g., $(MgO)_n^+$, $(MgO)_nMg^+$, Ca_nO, Ba_nO_m [73,74,75,76]. High peak intensities in mass abundance spectra or variations in ionization energies cannot be related to electronic shell closing but rather to structural or geometric effects. In particular, the segregation model, which holds relatively well for doped alkali clusters, does not seem to be valid for alkaline-earth oxides. Studies on the third main group metal oxide clusters, i.e., Al_nO_m, Ga_nO_m, In_nO_m, [77] report an enhanced stability for cluster ions containing an even number of electrons, even for the oxygen-rich ones. Nevertheless, as for their pure metal counterparts, their size dependent properties seem to be governed by the interplay between electronic and geometric factors. Among the species doped by a single electronegative atom, enhanced stabilities or electronic shell closing effects in their electronic properties (ionization energies, photoelectron spectra) have been reported for Al_7N, Al_7C^-, In_7O^+, $Al_{12}C$, $Al_{12}B^-$ [78,79,80,81] which can be related to electronic shell closing numbers 26 and 40 that show up in electronic shell models modified for electronegative central dopant atoms as discussed above. Moreover the enhanced stabilities of the 13-atom species $Al_{12}C$, $Al_{12}B^-$ are due to the combined effect of a closed electronic structure and a highly symmetric dopant-encapsulated icosahedral structure [82]. As an example of the 8 atom species, the electronic structure resulting from quantum chemical calculations of the endohedral In_7O^+ C_{3v}-isomer, orbitals and energy level sequence, is shown in Figure 8. The pattern shows a closed electronic shell structure with a large HOMO-LUMO gap of 2.3 eV and 26 electrons in 13 delocalized orbitals. Because of the rather spherical shape of the C_{3v}-isomer, the orbitals, to a certain extent, resemble the *s*, *p*, and *d* type spherical harmonics. Notice that both the energy gaps (shell closings) at 10 and 26 electrons are present in the modified two-step jellium model (Figure 5) discussed above for a central depression of the potential due to a central electronegative

dopant. The latter example illustrates how valuable simple spherical shell models are in predicting the basic electronic properties of a large variety of clusters and, the other way round, how these basic features remain present in the output of more sophisticated quantum chemical computations.

More recently, iodized aluminum clusters attracted a lot of attention in the quest for clusters with coincident closures of their electronic and geometric shells that can act as superatoms. The observation of the very stable $Al_{13}I^-$ cluster evidences the superhalogen character of Al_{13}, lacking one electron to form a 40 electron closed shell structure [83]. The stability and reactivity of the $Al_{13}I_x^-$ and $Al_{14}I_x^-$ series also is interpreted in terms of a simple spherical shell model and their potential use in superatom chemistry was addressed [84].

It should be noted that, apart form the doped main group metal clusters, numerous studies are available on transition metal oxide clusters. Because of the open *d* shell of the transition metal atoms, size-dependent properties of such clusters are governed by a complex interplay between electronic and structural aspects and are impossible to describe using simple electronic and geometric shell models.

4.2 Transition-metal doped noble metal clusters

Size dependent properties, e.g., stability patterns in mass abundance spectra, ionization energies, dissociation energies, of coinage metal (Cu, Ag, and Au) clusters can be described by theoretical models based on the dominating role of the number of delocalized valence electrons as in the case of for example simple alkali metal clusters, because they have a completely filled *d* shell and one valence *s* electron in the atomic ground state. On the other hand, a simple electronic shell model cannot be applied for clusters comprised of more complex atoms, such as open *d* shell transition metals. The *d* electrons of transition metals engage in more localized, directional bonding than the outermost *s* and *p* electrons of simple metals. With the study of transition metal doped noble metal clusters, the interaction between localized bonds and free electrons can be examined.

The radial extent of the open *d* shell is an important parameter. The extent decreases along a row (e.g., from Sc to Ni) and increases with the increasing row number (e.g., from Sc to Ac).

Large dopant *d* orbitals can hybridize strongly with host *s* or *d* electrons. This increases the tendency toward itinerant *d* behavior, such that the *d* electrons should be considered as free electrons. On the other hand smaller *d* orbitals do not interact strongly with the host electrons. A photofragmentation mass spectrometry study of Au_n clusters doped with 3*d* transition metal atoms demonstrated that the light dopants (Sc, Ti) contribute both their 4*s* and 3*d* electrons to the cloud of itinerant electrons, while for the heavier elements (Cr, Mn, Fe, Co, Ni) only the 4*s* electrons are delocalized [85,86]. The interpretation was supported by the shapes of the highest occupied molecular orbitals found in density functional theory calculations [87,88]. The difference between the light and heavy dopants is related to the different size of *d* electron wave functions resulting in a stronger or weaker hybridization with the Au valence electrons. Moreover, if only the dopant *s* electrons are itinerant, the energetic competition between $3d^x4s^2$ and $3d^{x+1}4s^1$ dopant configurations is crucial. Most often the monovalent or divalent character agrees with the atomic ground state configuration of the free atom. However, the host environment may alter energetic preferences, e.g., Cr ($3d^5 4s^1$) is divalent in Au_n, Ni ($3d^8 4s^2$) is monovalent in Na_n, Cu_n, and Au_n [85,89], and Co ($3d^7 4s^2$) acts monovalent in Al_n while it is divalent in Au_n [85,90].

The stability patterns of the doped Au_n clusters mentioned above were discussed on the basis of a simple phenomenological shell model, taking into account only the electronic structure of the dopant atom. In several doped systems, e.g., $Au_{16}Sc^+$, $Au_{15}Ti^+$, $Au_{17}X^+$ (X = Cr, Mn, Fe, Co), $Au_{18}Ni^+$, or $Au_{16}Y^+$, the magic number 18 manifests itself as a strong shell closing, at the cost of 20, which is observed for pure Au_n clusters. As an example the photofragmentation spectrum of cationic Au_NY^+ clusters is given in Figure 9 [42]. The most pronounced feature in this mass spectrum is the intense signal recorded for $Au_{16}Y^+$, which is a direct fingerprint of the high stability of this species relative to neighbouring cluster sizes and relates to the closed electronic shell structure formed by the 18 valence electrons.

Besides a dopant dependence of the electronic structure, this study also indicates how the cluster shape can be modified by proper doping, resulting in new magic numbers that correspond to planar cluster species. While Au_9^+ is observed as a magic cluster containing 8 delocalized electrons in the case of pure gold cationic clusters, the mass abundance spectra of Au_nX^+ (X = Cr, Mn, Fe, Co, Zn) feature enhanced stability for Au_5X^+ systems, which is

ascribed to a planar triangular ground state structure in combination with six delocalized electrons being a magic number for 2D systems [86,91,92]. The experiments showed very little evidence for an enhanced stability of Au_7X^+ species, which should contain eight valence electrons. The electronic structure and magnetic properties of MAu_6^- (M = Ti, V, Cr) have been investigated experimentally using photoelectron spectroscopy and density functional theory calculations [93]. It is found that all MAu_6^- and MAu_6 clusters possess a planar structure, in which the transition metal atom is located in the center of a Au_6 ring and carries large magnetic moments. Meanwhile, also homogeneous gold clusters are known to be planar up to fairly large sizes, depending on their charge state, due to relativistically enhanced *s-d* hybridization [94,95,96].

Transition metal doped gold clusters not only have been studied because of the fundamental interest in understanding the interplay between geometric and electronic effects in bimetallic clusters. At the same time, the peculiar optical and catalytic properties observed for pure gold clusters [97] triggered the search for highly stable transition metal doped gold clusters, since the additional degree of freedom inherent to bimetallic clusters can enhance the chemical versatility for tuning the electronic and geometric properties of gold-based clusters and related potential applications.

The pioneering example in this respect is the icosahedral $Au_{12}W$ cluster [98,99,100,101]. In the latter, the W dopant atom has large *d* orbitals and delocalizes both its two 6*s* and 5*d* electrons. This cluster has a compact geometry with the tungsten atom in the center of a cage and a closed-shell electronic structure with a large HOMO-LUMO gap, confirmed experimentally by photoelectron spectroscopy [99]. $Au_{12}W$ is stabilized for three complementary reasons: (i) relativistic effects that strengthen the radial W – Au and the covalent Au – Au bonds, (ii) aurophilic attraction in the periphery, and (iii) a closed electronic structure with 18 valence electrons [98]. The electrons occupy orbitals with a_g, t_{1u}, and h_g symmetry that show similarities to the 1*s*, 1*p*, and 1*d* spherical levels (the shapes are somewhat more complex because of strong gold *s-d* hybridization). Meanwhile, the isoelectronic species $MoAu_{12}$, VAu_{12}^-, $NbAu_{12}^-$, and $TaAu_{12}^-$ have been produced and characterized experimentally by photoelectron spectroscopy, while the theoretically predicted isoelectronic cation $ReAu_{12}^+$, however, has not. It should be noted that icosahedral $Au_{12}Pd$

has been prepared chemically in solution [102] and characterized computationally [103] before $Au_{12}W$, however, this is not a magic closed electronic shell cluster.

Although $Au_{12}W$ was originally thought to be stiff, a careful study of its vibrational properties [100] actually showed it to be very soft in the angular motions of the W-Au bonds, a property shared by many systems with Au-Au bonds [96]. Another indication of this softness is that $Au_{12}W$ completely deforms when placed inside a Si_{60} cage [104]. As can be seen in Figure 10, the magic $Au_{12}W$ cluster interacts strongly with Si_{60} and stabilizes the caged structure. This interaction completely destroys the icosahedral geometry of $Au_{12}W$ and the symmetry of the Si_{60} cage.

A number of fullerene-like pure gold cages of different sizes, e.g., Au_{26} [105], Au_{32} [106], Au_{42} [107], Au_{50} [108], have been predicted. More recently experimental evidence for the existence of hollow Au_n (n = 16-18,20) cages was deduced from PES data [109,110]. Combined calculations suggest that these hollow Au_n (n = 16-18) cages can easily accommodate a guest atom with very little structural distortion to the host cages. Indeed, a number of highly stable gold-covered bimetallic clusters, $M@Au_n$ (n = 9-17) obeying the 18 electron rule, were predicted computationally [111,112]. It is found that starting from n = 9, the hetero-atom (M) prefers to be entirely surrounded by gold atoms to attain the lowest energy structure. In particular, WAu_{12}, $ZrAu_{14}$, $ScAu_{15}$, and YAu_{15} would stand out in stability, as concluded by their high binding energy per atom (> 2.40 eV) as well as a large HOMO-LUMO gap (> 1.70 eV). The latter may explain the very large abundances observed experimentally for the isoelectronic cations YAu_{16}^+, and $ScAu_{16}^+$, in the photofragmentation studies mentioned above [42,85]. Note that the endohedral geometry of these clusters confirms the shell model interpretation based on a hump at the center of the phenomenological potential.

In another theoretical study $SiAu_{16}$ is found to be a stable dopant-encapsulated tetrahedral, geometrically robust cage, satisfying the 20-electron shell closing of the conventional jellium model [113].

To end the overview of gold-based binary systems we want to mention a recently reported 'eccentric' computational example of a molecular gold-plated diamond C_5Au_{12} cluster [114]. A tetrahedral C_5 radical (unit of the diamond crystal lattice) is encapsulated in a Au_{12} layer of matching geometry, with the Au atoms in positions correlating to the pattern of bonds of the

sp^3-hybridized carbons, resulting in distorted icosahedral and octahedral ground state geometries being nearly iso-energetic.

To our knowledge, studies on binary silver based clusters are much less numerous compared to gold. However, the 3*d* transition metal doped gold clusters study mentioned above, has been extended to silver clusters [115,116,117,118]. The stability patterns of Ag_nX^+ (X = Sc, Ti, V, Cr, Mn, Ni, Cu) reflect an electronic shell structure with dopant dependent magic numbers. The open 3*d* shell transition metal dopant is considered to contribute its 4*s* electrons (for Cr up to Ni) or its 3*d* and 4*s* electrons (Sc and selected sizes for Ti and V) to a cloud of itinerant electrons. Among the clusters containing 18 valence electrons, remarkable stabilities are observed for $Ag_{16}Sc^+$, $Ag_{15}Ti^+$, $Ag_{14}V^+$, similar to doped gold. The size dependent electron delocalization is attributed to the small energy difference between $3d^x4s^2$ and $3d^{x+1}4s^1$ atomic configurations of the dopant atoms. Contrary to doped gold clusters, Ag_5X^+ (X = V, Cr, Mn, Fe, Co) species do not show up as particularly stable and as such no evidence is found for the existence of 2D electronic shell closures in doped silver clusters [116]. Nevertheless, a density functional theory study revealed that the Ag_5X^+ (X = Sc, Ti, V, Cr, Mn, Fe, Co, and Ni) clusters prefer planar or semi-planar C_{5v} symmetries, significantly flattened compared to the 3D tripyramidal geometry found for pure Ag_6^+, indicating that the transition metal dopant enhances the planar character of the clusters [117]. In all low energy isomers the dopant occupies a highly coordinated site. Also, a high spin magnetic moment is found on the dopant atoms, only slightly lower than the free atom value, which is a signature for limited silver 5*s*-dopant 3*d* hybridization. These results were recently extended towards neutral and anionic $Ag_5X^{0,-}$ (X = Sc, Ti, V, Cr, Mn, Fe, Co, and Ni) clusters [119]. In Figure 11 the ground state geometries of a few doped $Ag_5X^{+,0,-}$ and $Au_5X^{+,0}$ are compared with the geometries of Ag_6^+ and Au_6^+. Where both the bare gold and the doped gold clusters are planar, several three dimensional geometries are found for the doped silver clusters. However, most $Ag_5X^{0,+,-}$ clusters are seriously flattened compared to the bare $Ag_6^{+,0,-}$ geometries [119]. A comparison of the cationic Ag_5Fe^+, the neutral Ag_5Fe^0, and the anionic Ag_5Fe^- shows that also the charge state can have an important influence on the structure.

The most astonishing observation for 3*d* transition metal doped silver clusters is the strong stability of $Ag_{11}Fe^+$, $Ag_{10}Co^+$, and Ag_9Ni^+. Enhanced stabilities for the corresponding sizes

were not observed for doped gold clusters. These stabilities could be explained by an itinerant behaviour of both the 4*s* and 3*d* dopant atom electrons. In that case the Fe, Co, and Ni atom in $Ag_{11}Fe^+$, $Ag_{10}Co^+$, and Ag_9Ni^+ would delocalize 8, 9 and 10 valence electrons, respectively, yielding a total of 18 electrons, a magic number in the spherical shell model. Although unrealistic at first sight, this argumentation was confirmed by detailed quantum chemical calculations of the electronic and geometric structure of $Ag_{10}Co^+$. The latter was found to have a symmetric endohedral geometry (only slightly distorted from D_{4d}) with a closed 18-electron singlet electronic shell structure, implying that the magnetic moment on the cobalt atom is completely quenched. Hybridization of the atomic silver 5*s* levels with the cobalt 3*d* levels leads to the formation of delocalized molecular orbitals that resemble the spherical harmonic functions 1*s*, 1*p*, and 1*d*. This specific size and composition dependent behaviour is analogous to the screening electron cloud formation in magnetic-element-doped bulk metals and therefore can be interpreted as a finite-size precursor of the Kondo-system. It should be noted that a similar behaviour has been predicted in a number of highly symmetric transition metal doped noble metal clusters: $Cu_{12}Cr$ [120], $Ag_{12}Cr$ [121], $Au_{12}Cr$ [122], and $Au_{12}W$.

By investigating the preferable dissociation channel after laser heating and subsequent fragmentation of mixed silver-cobalt particles, it was recently shown that in clusters containing mainly silver, the cobalt sits at the cluster center and fragmentation proceeds by the evaporation of silver surface atoms [118]. In clusters containing mainly cobalt, silver atoms also locate at the periphery and are more weakly bound to the cluster than the cobalt surface atoms. Moreover, the special stability of $Ag_{10}Co^+$ was demonstrated in these delayed fragmentation studies, as is shown in figure 12.

4.3 Transition-metal/metal doped group IV

Silicon is one of the most important materials used in microelectronics industry. Stimulated by the discovery of carbon fullerenes and, later on, carbon nanotubes, many efforts are made to search for similar silicon cage structures. However, although silicon shares the diamond structure with carbon, both elements behave differently in clusters. Carbon prefers sp^2 bonding, which appears in the structure of graphite, while silicon prefers sp^3 bonding. The

latter makes it difficult to form stable hollow cage structures such as C_{60}. A possible approach to stabilize hollow silicon cage structures was proposed by Jackson and coworkers [123]. Inspired by small C_{28} fullerenes that were stabilized by a central guest atom as for example in UC_{28} [124], applying the same idea, a strikingly large binding energy (15.2 eV) is obtained for the icosahedral Si_{20} cage, which is not a stable isomer for the bare cage, by putting a Zr atom inside.

About ten years earlier, Beck already discovered stable silicon cluster – metal atom compounds of remarkable but identical stoichiometries for three different transition metal dopants, namely chromium, molybdenum, and tungsten: MSi_{15} and MSi_{16} (M = Cr, Mo, and W) [125]. However, despite a valuable attempt based on a topological model [126], the magic behaviour of these structures remained unexplained for more than a decade until Kumar and Kawazoe computationally attributed the strong stability to dopant-encapsulated cage-like structures with large values of binding energy, highest occupied – lowest unoccupied molecular orbital (HOMO-LUMO) gap, and embedding energy of the dopant atom [127]. The magnetic moment of the dopants is completely quenched. An interesting property of these metal-encapsulated silicon clusters lies in the tunability of the band gap depending on the dopant atom. Metal dopants can enhance the symmetry of the host cluster or enlarge the HOMO-LUMO gap into the region of visible light.

Experiments on endohedral complexes involving metal atoms and non-metallic Si_n cages have demonstrated that $Si_{14}Hf$, $Si_{13}Ta$, $Si_{12}W$, and $Si_{11}Re$ clusters are magic [128]. Calculations on $Si_{10}Fe$, $Si_{12}Cr$, and $Si_{12}W$ predict endohedral geometries (no icosahedra) with interesting electronic structures [128,129,130]. The central dopant atom in the Si_nX clusters has a $md^{18-n-2}(m+1)s^2$ electron configuration and interacts with all n Si atoms. If each Si atom is singly bonded to the central atom, this atom gets 18 electrons (18-n-2 from *d* orbitals, 2 from *s* orbitals, and n from the Si neighbors) in total. The transition metal dopant obtains a closed electronic structure, in accordance with the 18-electron rule for *d*-block organometallic complexes. This rule states that the number of nonbonded electrons at the metal plus the number of electrons in the metal-ligand bonds should be 18 [131]. At the same time, 3 valence electrons are left for each Si atom, making it possible to form a Si polyhedron without dangling bonds [128,130]. So, these clusters are not stabilized by the formation of closed

jellium states but by the 18-electron rule for the metal dopant in combination with a covalently bonded Si cage.

Most recently, Nakajima and coworkers [132] reported the selective formation of highly stable MSi_{16} (M = Sc, Ti, and V) clusters by fine tuning the laser vaporisation source conditions (Figure 13). VSi_{16}^+, $TiSi_{16}$, and $ScSi_{16}^-$ are electronically closed. Similar to the case of Al_{13} discussed above, the reactivity of MSi_{16} towards F_2 was examined. The formation of $VSi_{16}F$ suggests that VSi_{16} is an alkali atom-like species and $ScSi_{16}^-$ is suggested to behave like a superhalogen, as observed for Al_{13}^- [83,84].

The initial interest in doped silicon systems [133,134,135,136,137,138,139,140,141,142,143, 144,145,146,147,148] rapidly extended to its higher mass congeners [52,149,150,151, 152,153]. Notable examples, computationally predicted, are metal-encapsulated icosahedral superatoms of germanium and tin, $ZnGe_{12}$ and $CdSn_{12}$, with large HOMO-LUMO gaps or $MnGe_{12}$ and $MnSn_{12}$, with high magnetic moments. A number of typical endohedral close packed structures for metal encapsulated group IV clusters $X@M_n$ in the size range n = 10, 12, 14 – 16 are shown in Figure 14 [154]. Experimental studies however, are far more scarce than for doped silicon species [53,125,132,155,156,157,158]. A mass spectrometric study on $Co_xGe_n^-$, $CoSn_n^-$, and $CoPb_n^-$ anions reports an enhanced stability for $CoPb_{10,12}^-$ [159].

Mass spectrometric characterization of Pb_nAl^+ clusters produced in a laser vaporization source showed an extremely large abundance for $Pb_{12}Al^+$ species and to a lesser extent for $Pb_{10}Al^+$ [160] (Figure 15). Structural analysis with density functional theory revealed an icosahedral ground state for $Pb_{12}Al^+$. A large HOMO-LUMO gap (3.1 eV) and a large energy difference relative to the second most favorable isomer (1.96 eV) were further evidence for the particular stability of this system. The 50 valence electrons occupy 25 MO's, which are delocalized over the entire cluster. The orbitals resemble spherical shell model states, but the level ordering is different. The 50-electron shell closing originates from the crystal-field splitting of the high angular momentum levels according to the icosahedral symmetry of the cluster. The radial orbitals that point towards the positively charged lead atom centers are lower in energy, while tangential MO's with maximum density in between the atoms are less favorable. The splitting of the 1*g* level results in a very pronounced HOMO-LUMO gap at the 50 electron occupancy. Almost at the same time $Pb_{12}Pt^{2-}$ clusters, which are isoelectronic with

$Pb_{12}Al^+$, were prepared chemically in high yield (60%) [161]. Meanwhile, also the size-dependent stability and electronic and geometric properties of the lower mass congeners AlX_n^+ (X = Si, Ge, Sn) have been investigated [162] and related species like $MPb_{10,12}^{2-}$ (M = Ni, Pt, Pd) as well as Pb_{12}^{2-} and Sn_{12}^{2-} have been identified experimentally [163,164,165]. Recently, the superalkali character of the neutral MPb_{12} (M = B, Al, Ga, In, and Tl) was studied computationally [166].

A more extended experimental study of the size, host, and dopant dependent stability of metal doped semi-metal clusters MS_n (M = Cr, Mn, Cu, Zn; S = Si, Ge, Sn, Pb) partly covers the large variety of metal dopant – group IVA host combinations that have been accessed theoretically in literature [167]. Enhanced stabilities are observed for $MSi_{15,16}$ and $MGe_{14\text{-}16}$ with M = Cr, Mn but not for Cu and Zn doped clusters, which seems to confirm the that the possibility of *d* band filling of the dopant atom with dangling bond electrons from the surrounding Si_n and Ge_n cages is crucial in obtaining stable endohedral cage structures. Similar to the examples discussed above, relatively enhanced abundances are found for the MPb_{12} species which probably relate to close-packed icosahedral structures. The situation is less straightforward for doped Sn_n clusters, but the reported data experimentally confirm the theoretically predicted special stability of the metal doped magic magnetic superatom $MnSn_{12}$. Finally, a general principle for designing stable highly symmetrical clusters was proposed [162]. The approach takes advantage of both the extra stability provided by an optimal electronic configuration of the cage and the good geometrical balance between the outer cage and the endohedral atom, as schematically represented in Figure 16. In this case the optimal character of the electronic configuration of the cluster is probed through its aromatic properties [168]. The applicability of this design principle was confirmed by gas phase experimental observations on group IV element cages with endohedral Al atoms and also was illustrated by many literature examples of diverse systems.

5. Summary & Outlook

Proper choice of the constituent atoms provides a handle to tune the properties of mixed clusters. Indeed, physical (optical, electronic, magnetic…) and chemical (reactivity, catalytic

activity…) properties not only depend on the cluster size, but they obviously are determined by the choice of constituent atoms. Moreover, several recent examples outlined in this review have demonstrated that tuning the atomic building blocks allows forming specific clusters with strongly enhanced stability. Shell model concepts developed now 20 years ago based on shells of electrons and shells of atoms are playing a key role in this context. If highly symmetric structures with a well defined geometry coincide with closed shells of delocalized valence electrons of properly chosen constituent atoms, doubly magic species are demonstrated to exist. With still a large number of binary and even more ternary cluster systems to explore, many more sizes and compositions may result in clusters with enhanced stability.

Since in several cases these species were shown to have atom-like characteristics, their use as building blocks for new materials can be envisaged. Therefore one can expect that engineering the properties of these clusters building blocks by size and composition will lead to the creation of new materials structured on a nanometer scale with tailor-made properties.

Figures

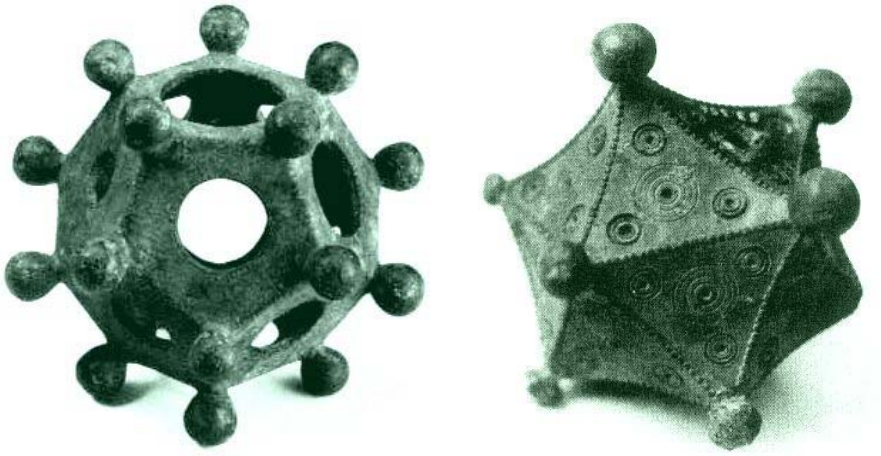

Figure 1: Highly symmetric bronze objects dating back to the Gallo-Roman time, dodecahedron (left) and icosahedron (right), of which a few tens have been retrieved all over Europe [1].

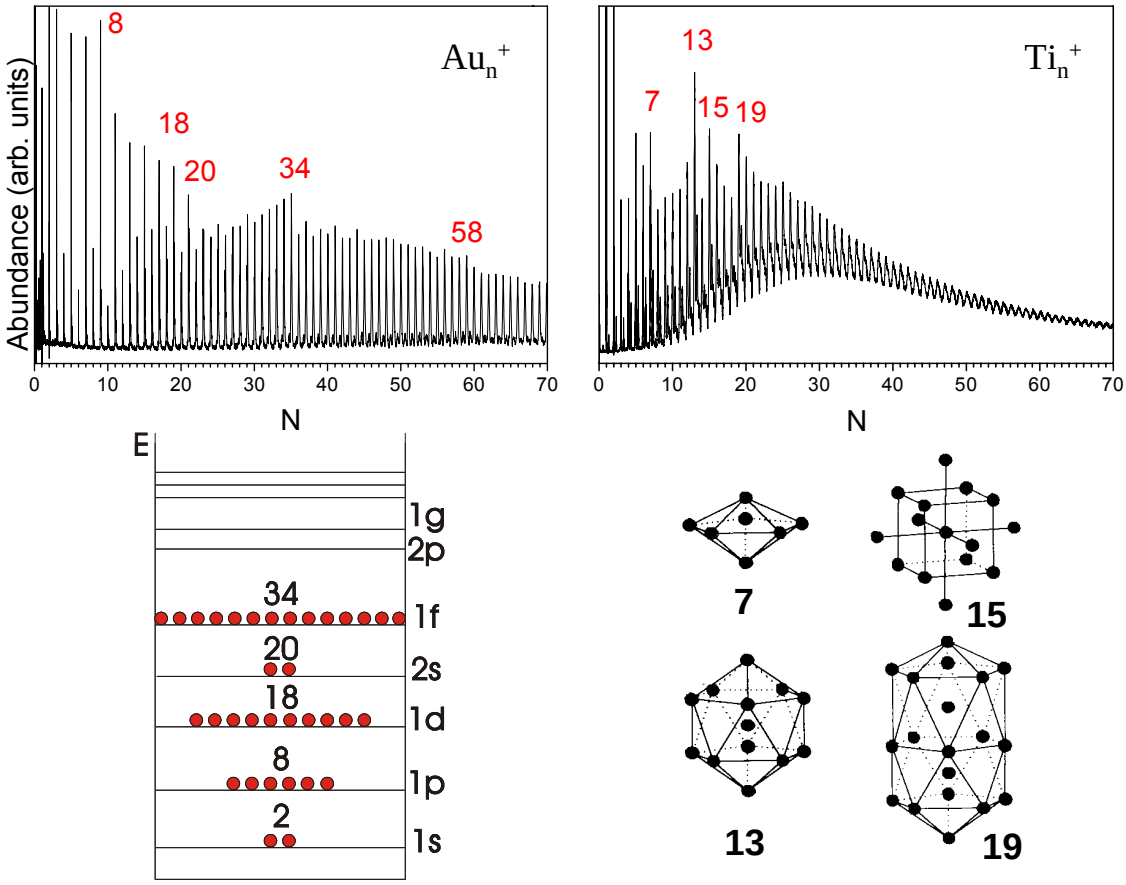

Figure 2: Mass abundance spectra of gold (left) and titanium (right) clusters, showing electronic and geometric magic numbers, respectively. The lower panel shows a schematic representation of the sequence of spherical electronic shells, as it applies to gold clusters, and a number of small symmetric geometric structures, that apply to titanium clusters.

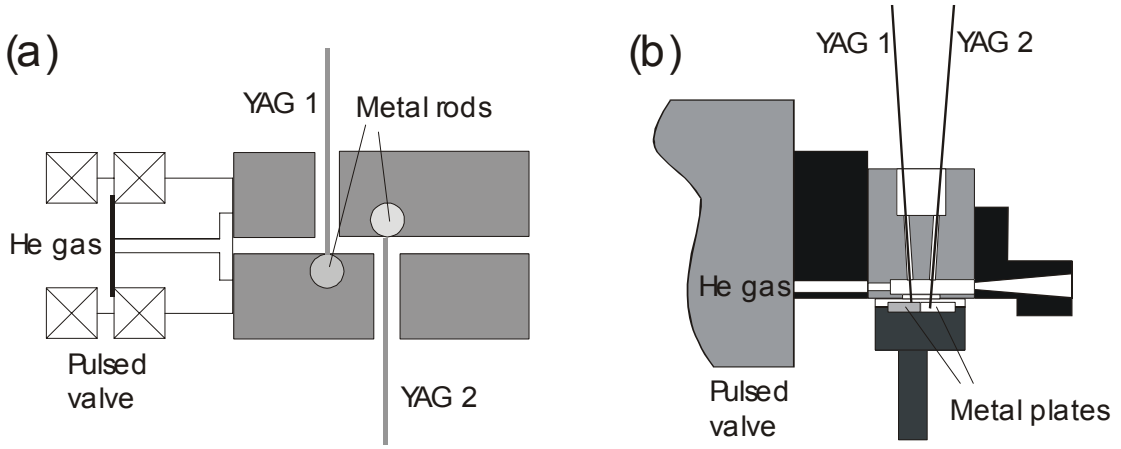

Figure 3: (a) Schematic diagram of the original binary laser vaporization source developed by Kaya and coworkers using two separate metal rods [18]. (b) Schematic diagram of the binary laser vaporization source constructed by Lievens and coworkers using two different metal plates [19]. In both cases the metal targets are vaporized by the second harmonics (532 nm) of two Nd^{3+}:YAG lasers and the He carrier gas (5-10 atm, 99,9999% purity) enters the source through a pulsed gas valve. The plumes of evaporated material are mixed with the inert carrier gas, collisions occur and cluster formation starts. The mixture of gas, atoms and clusters expands adiabatically into the vacuum through the nozzle opening. Hereby, the clusters are further cooled and cluster formation stops because of the rapidly decreasing density.

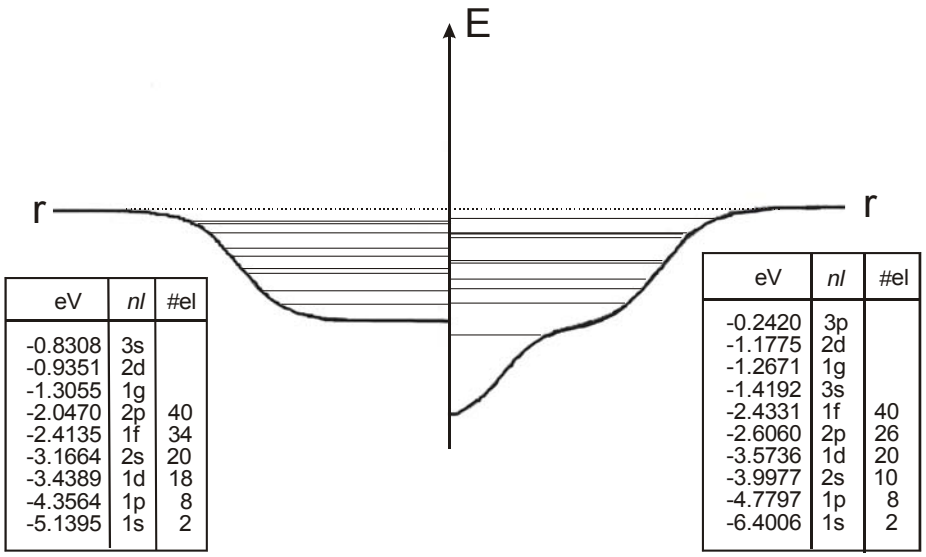

eV	*nl*	#el
-0.8308	3s	
-0.9351	2d	
-1.3055	1g	
-2.0470	2p	40
-2.4135	1f	34
-3.1664	2s	20
-3.4389	1d	18
-4.3564	1p	8
-5.1395	1s	2

eV	*nl*	#el
-0.2420	3p	
-1.1775	2d	
-1.2671	1g	
-1.4192	3s	
-2.4331	1f	40
-2.6060	2p	26
-3.5736	1d	20
-3.9977	2s	10
-4.7797	1p	8
-6.4006	1s	2

Figure 4: Wood-Saxon potential for Na_{40} and a modified Wood-Saxon potential for $Na_{38}Mg$ (both clusters have a total of 40 valence electrons). Their respective eigenstates are compared with identical energy scale to illustrate the modification of the potential due to the incorporated heteroatom. The heteroatom induces a depression at the center of the well. This leads mainly to a selective stabilization of *ns* states (states with angular momentum zero) and in a weaker fashion for *p*>*d*>*f*… In the tables the energy, principal and angular momentum quantum numbers (*n* and *l*), and the sum of valence electrons for the calculated eigenstates are listed for Na_{40} and $Na_{38}Mg$, respectively. The difference in the level order is due to a 1*d*/2*s* level inversion. (Reproduced with permission from ref. 36.)

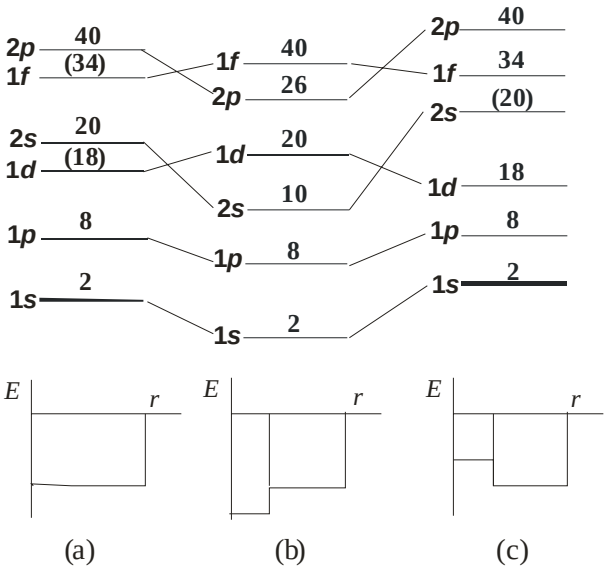

Figure 5: Schematic representation of the single particle energy levels in the standard jellium model (a) and in the two-step jellium model with a depression (b) and an increase (c) in the central part of the background potential. Note the lowering of the 2*s* and the 2*p* levels in (b) causing the magic numbers 10 and 26, and the lifting of the 2*s* level in (c) enhancing the magic number 18. (Reproduced with permission from ref. [47].)

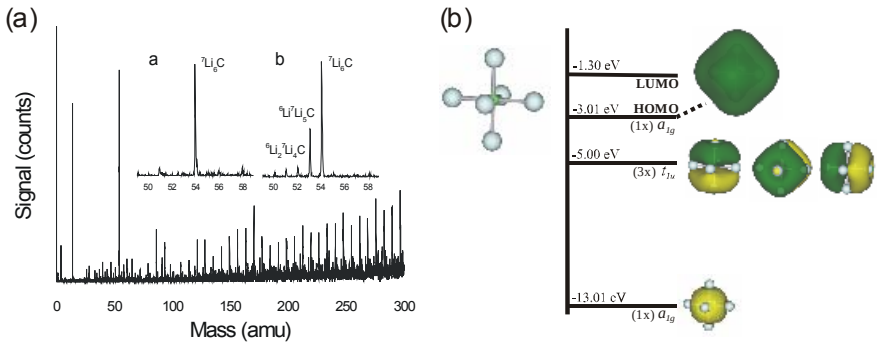

Figure 6: (a) Mass abundance spectra of doped Li clusters ionized with photons of 6.4 eV, employing isotopically enriched ^{7}Li as a vaporization target. Inserts: (a) selected mass region around Li_6C, and (b) same mass region as (a) employing natural ^{6,7}Li metal. (b) Ground state geometry, energy level scheme, and orbitals of the octahedral Li_6C from a density functional theory calculation. The ten valence electrons of Li_6C occupy the five depicted molecular orbitals. The two lowest energy electrons are located around the central C atom in an orbital with a_{1g} symmetry (1*s* type) . The ionic bonds of all Li atoms to the C atom consume six electrons, located in triple degenerate t_{1u} oribtals (1*p* type). The highest occupied molecular orbital of a_{1g} symmetry (2*s* type) contains the two remaining electrons that are located on a far extended orbit that is Li – Li bonding and Li – C antibonding.

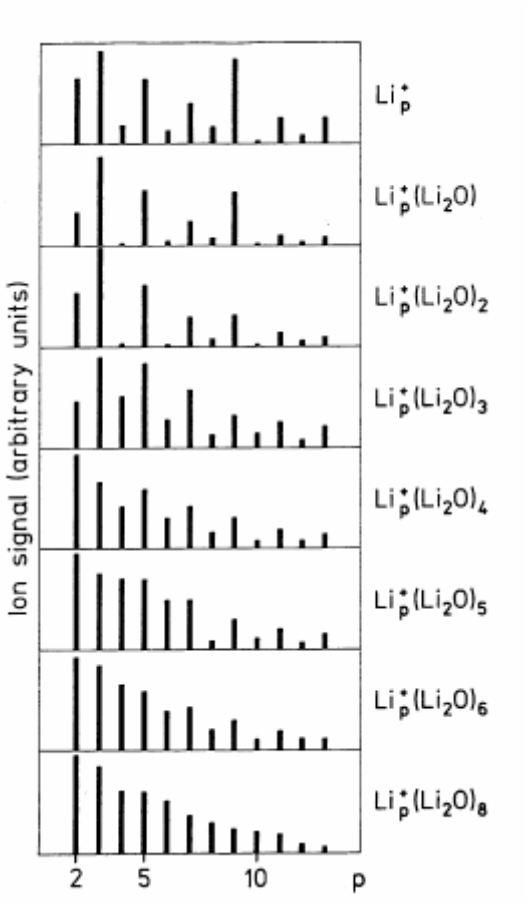

Figure 7: Mass spectra of evaporative sub-ensembles of $Li_p^+(Li_2O)_n$ versus p for several sizes of the ionic component $(Li_2O)_n$. Mixed lithium – lithium oxide aggregates are experimentally obtained from unimolecular evaporative cascades starting at metal rich $Li_p^+(Li_2O)_n$. The results provide evidence that the properties of the quantum metallic droplet, i.e., shell closing and odd-even alternation, are vanishing with increasing size of the oxide component. Notice, for example, the gradual disappearance of the enhanced abundance of the p = 9 species, which corresponds to the electronic shell closing for 8 delocalized valence electrons, with increasing ionic component n. (Reproduced with permission from ref. 72.)

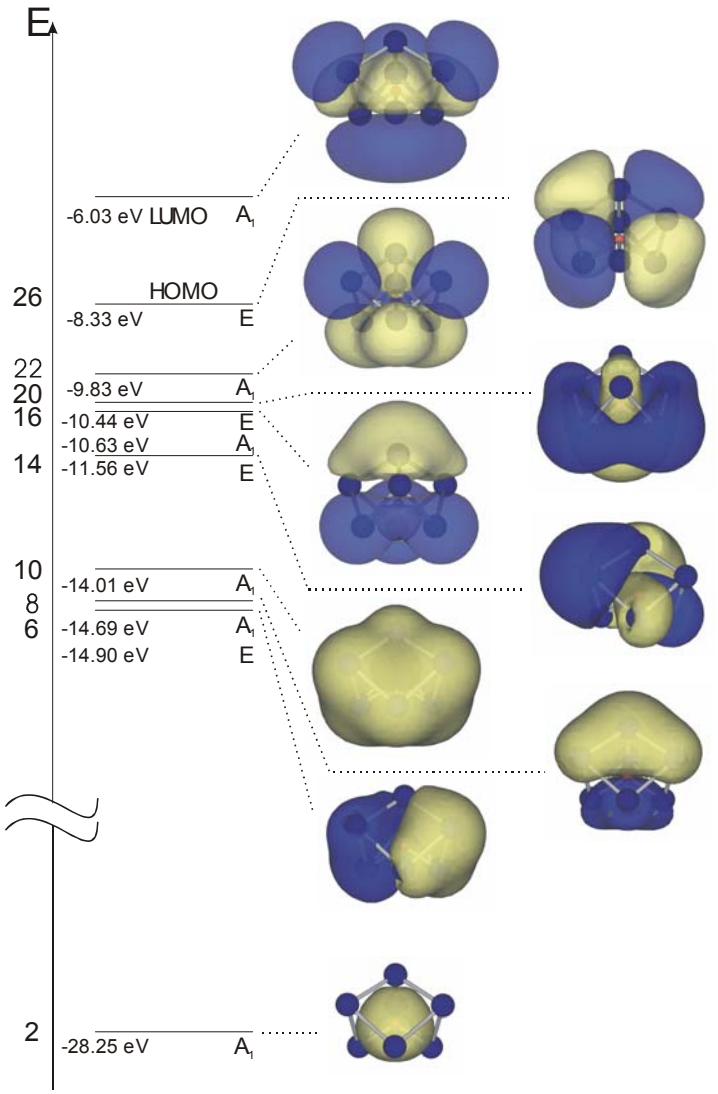

Figure 8: Energy level sequence and corresponding orbitals of the C_{3V} ground state isomer of In_7O^+, computed using density functional theory [81], showing 26 electrons in 13 delocalized orbitals and a large HOMO-LUMO gap of 2.3 eV confirming its magic electronic character.

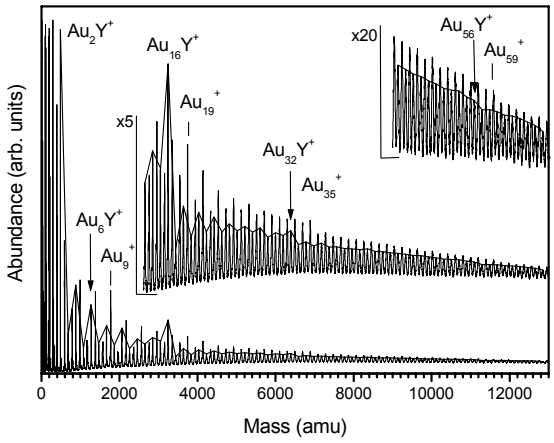

Figure 9: Mass abundance spectrum of $Au_nY_m^+$ clusters after photofragmentation. The solid line connects the Au_NY^+ species. Steps in abundance are observed at N = 2, 6, 16, 32, and 56. The pronounced pattern results from cooling by fragmentation and can be explained by the enhanced stability related to electronic shell closings for 2, 8, 18, 34, and 58 delocalized valence electrons 42. Recent computational studies predict an endohedral fullerene-like structure for the isoelectronic $Au_{15}Y$ and $Au_{15}Sc$ clusters with enhanced stability [112]. (Reproduced with permission from ref. 42.)

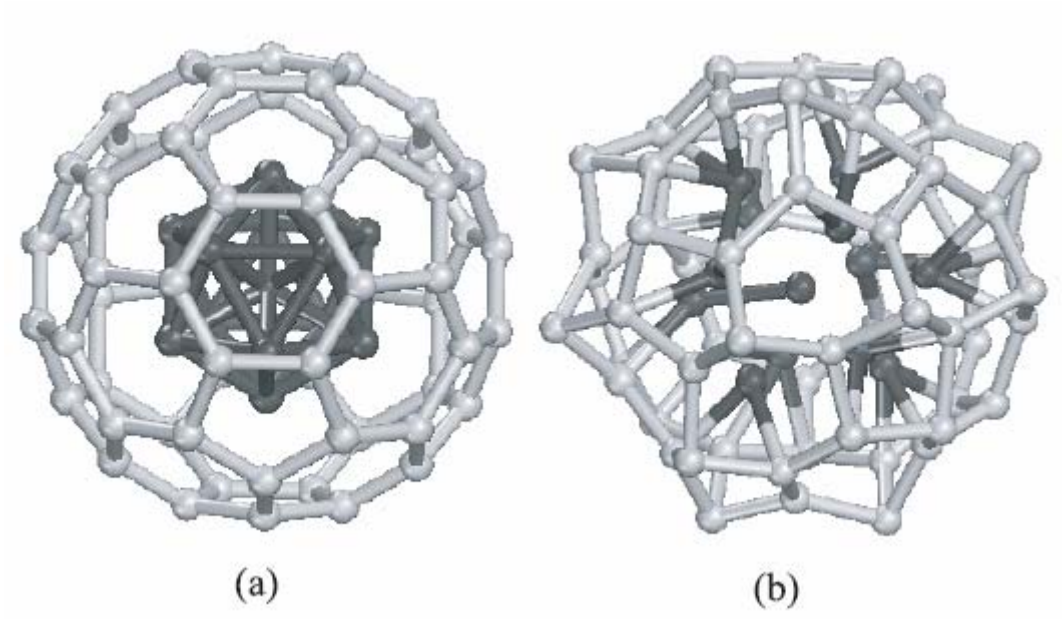

Figure 10: The initial (a) and optimized (b) geometries of $Au_{12}W$ in Si_{60}. The magic $Au_{12}W$ cluster is chemically active in Si_{60} and strongly interacts with the cage, resulting in a large energy gain, stabilization, and major deformation of both the doped gold cluster and the Si_{60} cage. (Reproduced with permission from ref. 104.)

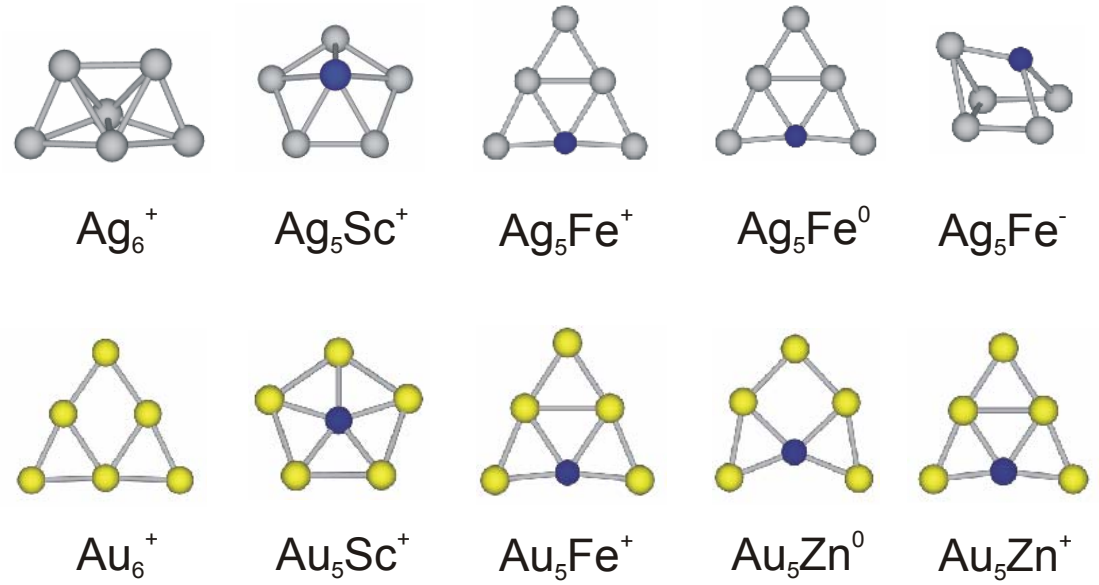

Figure 11: Ground state geometries of Ag_6^+ [117], Ag_5Sc^+ [117], Ag_5Fe^+ [117], Ag_5Fe^0 [119], Ag_5Fe^- [119], Au_6^+, Au_5Sc^+ [92], Au_5Fe^+[92], Au_5Zn^+ [91], and Au_5Zn^0 [91] clusters obtained with density functional theory.

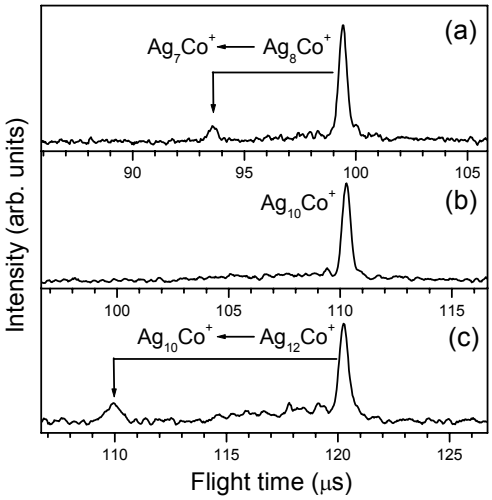

Figure 12: Delayed fragmentation spectra of Ag_8Co^+ (a), $Ag_{10}Co^+$ (b), and $Ag_{12}Co^+$ (c). The main fragmentation channel is labeled and appears to be size dependent. Ag_8Co^+ decays mainly by neutral silver evaporation. This is also the main dissociation channel for most other cluster sizes [see ref. 118 for more details]. However, $Ag_{10}Co^+$ does not show any delayed fragmentation, which is consistent with the high stability of this cluster [115]. For $Ag_{12}Co^+$ the main dissociation channel is the evaporation of a silver dimer, to create the stable $Ag_{10}Co^+$. The successive evaporation of two silver monomers is not very likely, since this would require the presence of a significant amount of $Ag_{11}Co^+$ fragments.

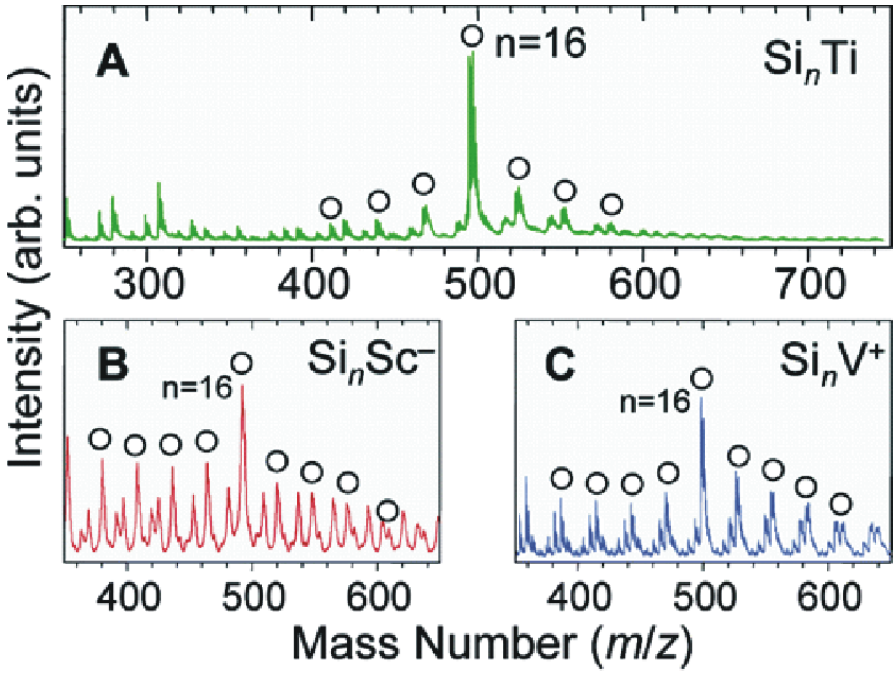

Figure 13: Mass spectra showing size-selective formation of (A) $TiSi_{16}$ neutrals, (B) $ScSi_{16}$ anions, and (C) VSi_{16}. (Reproduced with permission from ref. 132.)

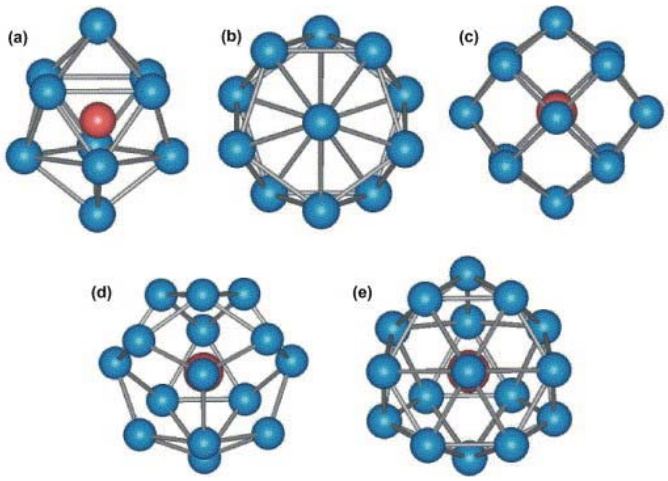

Figure 14: Closed packed structures of M encapsulated clusters of X atoms: (a) bicapped tetragonal anti-prism for $Be@Si_{10}$, $Ni@Ge_{10}$, and $Pt@Sn_{10}$, (b) icosahedral $Be@X_{12}$, $Mn@X_{12}$ (X = Ge and Sn), $Al^{+}@Pb_{12}$, $Pt^{-2}@Pb_{12}$, $M@Au_{12}$ (M = Mo and W), $Cu@Al_{12}$, $Si@Al_{12}$, (c) cubic $M@Si_{14}$ (M = Fe, Ru, and Os) (d) Frank-Kasper FK-$M@Si_{15}$ (M = Cr, Mo, W), and (e) FK–$Ti@Si_{16}$ and $Zr@Ge_{16}$. The M atom is inside the cage. (Reproduced with permission from ref. 154.)

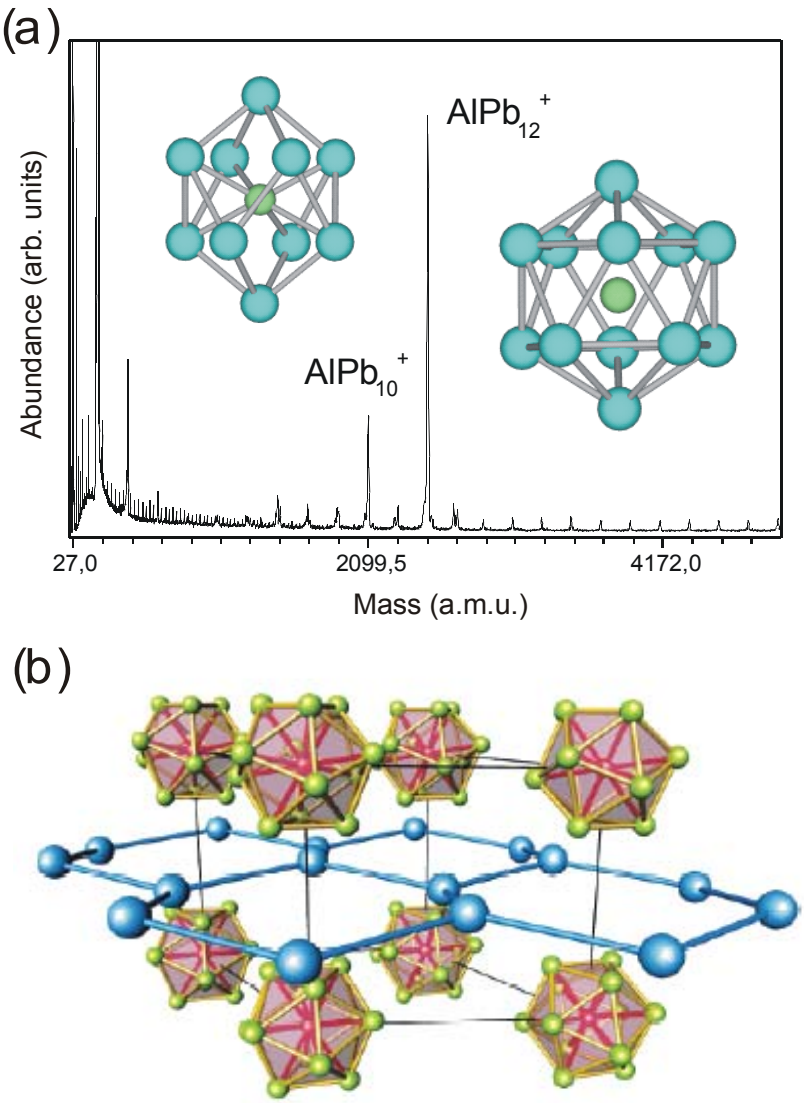

Figure 15: (a) Mass abundance spectrum of Pb_nAl^+ clusters featuring the exceptional stability observed for $Pb_{12}Al^+$ and, to a lesser extent, $Pb_{10}Al^+$. Their respective highly symmetric dopant encapsulated structures are shown. (b) Shematic illustration of MPb_{12}^{2-} ions (M = Ni, Pd, Pt) that are chemically produced in solutions in high yield as crystallized [K(2,2,2-crypt)]$_2$[M@Pb_{12}] salts. These crystallized salts form superlattices of cations and anions and are prototypes for assembled cluster materials. (Reproduced with permission from ref. 163.)

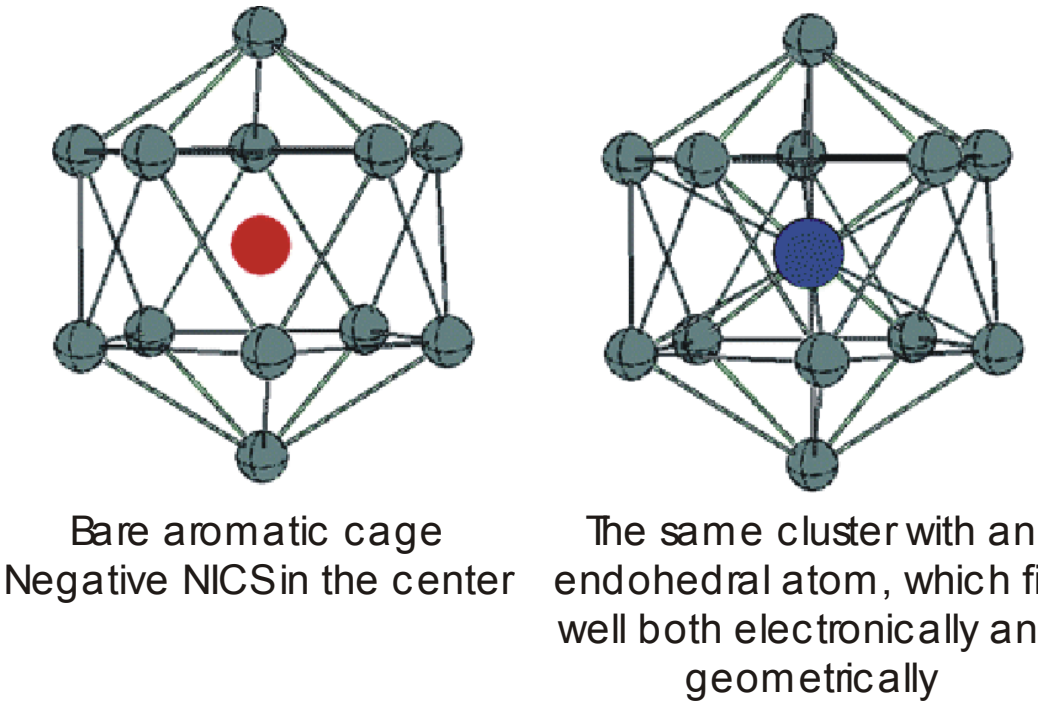

Figure 16: Schematic representation of the procedure to design a stable spherical cluster [162]. At first the character of the electronic structure of a bare cage is probed through its aromatic properties [168]. Hereby the number of electrons is adjusted by the appropriate choice of atoms and charges to achieve a closed electronic structure (significant aromatic character). The cage does not necessarily have to be a local minimum structure. Subsequently, the cage is filled with a dopant atom of suitable size and electronic structure (to maintain the electron count). Electron transfer and a degree of covalent bonding between the endohedral atom and the outer cage can further enhance the binding energy. The endohedral complex should be a local minimum with no imaginary vibrational frequencies. (Reproduced with permission from ref. 162.)

References

[1] G.W. Hart, Encyclopedia of Polyhedra, http://www.georgehart.com

[2] D.N. Marshall, Proceedings of the Society of Antiquaries of Scotland 180 (1976/77) 40.

[3] B. Artmann, American Mathematical Monthly 103 (1996) 132-133.

[4] O. Echt, K. Sattler, and E. Recknagel, Phys. Rev. Lett. 47 (1981) 1121-1124.

[5] A.L. Mackay, Acta Crystallogr. 15 (1981) 916-918.

[6] W.D. Knight, K. Clemenger, W.A. de Heer, W.A. Saunders, M.Y. Chou, and M.L. Cohen, Phys. Rev. Lett. 52 (1984) 2141-2143.

[7] H.W. Kroto, J.R. Heath, S.C. O'Brien, R.F. Curl, R.E. Smalley, Nature 318 (1985) 162-163.

[8] W.A. de Heer, Rev. Mod. Phys. 65 (1993) 611-676.

[9] T.P. Martin, J. Chem. Phys. 81 (1984) 4426-4432.

[10] T.P. Martin, J. Chem. Phys. 80 (1984) 170-175.

[11] C. Bréchignac, P. Cahuzac, R. Pflaum, J.P. Roux, 88 (1988) 3732-3735.

[12] T.G. Dietz, M.A. Duncan, D.E. Powers, R.E. Smalley, J. Chem. Phys. 74 (1981) 6511-6512.

[13] J.L. Rousset, A.M. Cadrot, F.J.C.S. Aires, A. Renouprez, P. Mélinon, A. Perez, M. Pellarin, J.L. Vialle, M. Broyer, J. Chem. Phys. 102 (1995) 8574-8585.

[14] W. J. C. Menezes, M.B. Knickelbein, Chem. Phys. Lett. 183 (1991) 357-362.

[15] H.T. Deng, B.C. Guo, K.P. Kerns, A.W. Castleman Jr., Int. J. Mass. Spectrom. Ion Processes 138 (1994) 275-281.

[16] L.R. Brock, A.M. Knight, J.E. Reddic, J.S. Pilgrim, M.A. Duncan, J. Chem. Phys. 106 (1997) 6268-6278.

[17] R.L. Wagner, W.D. Vann, A.W. Castleman, Rev. Sci. instrum. 68 (1997) 3010-3013.

[18] S. Nonose, Y. Sone, K. Onodera, S. Sudo, K. Kaya, J. Phys. Chem. 94 (1990) 2744-2746.

[19] W. Bouwen, P. Thoen, F. Vanhoutte, S. Bouckaert, F. Despa, H. Weidele, R.E. Silverans, P. Lievens, Rev. Sci. Instrum. 71 (2000) 54-58.

[20] A. Nakajima, K. Hoshino, T. Naganuma, Y. Sone, K. Kaya, J. Chem. Phys. 95 (1991) 7061-7066.

[21] K. Hoshino, T. Naganuma, K. Watanabe, Y. Konishi, A. Nakajima, K. Kaya, Chem. Phys. Lett. 239 (1995) 369-372.

[22] K. Koyasu, M. Mitsui, A. Nakajima, K. Kaya, Chem. Phys. Lett. 358 (2002) 224-230.

[23] C. Rosche, S. Wolf, T. Leisner, F. Granzer and L. Wöste, IS&T 48th Ann. Conf. Proc. 1994, 325-327.

[24] W. Pewestdorf, V. Bonačić-Koutecký, J. Koutecký, J. Chem. Phys. 89 (1988) 5794-5802.

[25] P. Fantucci, V. Bonačić-Koutecký, W. Pewestdorf, J. Koutecký, J . Chem.. Phys. 91 (1989) 4229-4241.

[26] P. v. R. Schleyer, E.U. Würthwein, J.A. Pople, J. Am. Chem. Soc. 104 (1982) 5839-5841.

[27] P.v.R. Schleyer, in *New horizons of quantum chemistry*, eds. P.O. Löwdin and B. Pullman (1983) 95-109.

[28] U. Röthlisberger, W. Andreoni, Chem. Phys. Lett. 198 (1992) 478-482.

[29] A. Rapallo, G. Rossi, R. Ferrando, A. Fortunelli, B.C. Curley, L.D. Lloyd, G.M. Tarbuck, R.L. Johnston, J. Chem. Phys. 122 (2006) 194308, and refs. therein.

[30] T. van Hoof, M. Hou, Eur. Phys. J. D 29 (2004) 33-38 and refs therein.

[31] M. Brack, Rev. Mod. Phys. 65 (1993) 677-732.

[32] W.D. Knight, W.A. de Heer, K. Clemenger, W.A. Saunders, Solid State Commun. 53 (1985) 445-446.

[33] M.M. Kappes, P. Radi, M. Schär, E. Schumacher, Chem. Phys. Lett. 119 (1985) 11-16.

[34] T.P. Martin, Angew. Chem. 98 (1996) 197-212.

[35] C. Bréchignac, P. Cahuzac, J.P. Roux, Chem. Phys. Lett. 127 (1996) 445-451.

[36] C. Yeretzian, J. Phys. Chem. 99 (1995) 123-130.

[37] C. Yeretzian, U. Röthlisberger, E. Schumacher, Chem. Phys. Lett. 237 (1995) 334-338.

[38] U. Heiz, A. Vayloyan, E. Schumacher, C. Yeretzian, M. Stener, P. Gisdakis, N. Rösch, J. Chem. Phys. 106 (1996) 5574-5585.

[39] K. Hoshino, K. Watanabe, Y. Konishi, T. Taguwa, A. Nakajima, K. Kaya, Chem. Phys. Lett. 231 (1994) 499-503.

[40] O.C. Thomas, W. Zheng, K.H. Bowen, J. Chem. Phys. 111 (2001) 5514-5519.

[41] M. Heinebrodt, N. Malinowski, F. Tast, W. Branz, I.M.L. Billas, T.P. Martin, J. Chem. Phys. 110 (1999) 9915-9921.

[42] W. Bouwen, F. Vanhoutte, F. Despa, S. Bouckaert, S. Neukermans, L.T. Kuhn, H. Weidele, P. Lievens and R.E. Silverans, Chem. Phys. Lett. 314 (1999) 227-233.

[43] X.P. Xing, Z.X. Tian, H.T. Liu, Z.C. Tang, Rap. Commun. Mass Spectrom. 17 (2003) 1411-1415.

[44] C. Yannouleas, P. Jena, S.N. Khanna, Phys. Rev. B 46 (1992) 9751-9760.

[45] S.B. Zhang, M.L. Cohen, M.Y. Chou, Phys. Rev. B 36 (1987) 3455-3458.

[46] C. Baladron, J.A. Alonso, Physica B 154 (1988) 73-81.

[47] E. Janssens, S. Neukermans, P. Lievens, Current Opinion in Solid State and Material Science, 8 (2004) 185-193.

[48] T. P. Martin, Physics Reports 273 (1996) 199–241.

[49] A.A. Shvartsburg, M.F. Jarrold, Chem. Phys. Lett. 317 (2000) 615-618.

[50] K.M. Ho, A.A. Shvartsburg, B. Pan, Z.Y. Lu, C.Z. Wang, J.G. Wacker, J.L. Fye, M.F. Jarrold, Nature 392 (1998) 582-585.

[51] J. Wang, G. Wang, J. Zhao, Phys. Rev. B 64 (2001) 205411.

[52] J. Lu and S. Nagase, Chem. Phys. Lett. 372 (2003) 394-398.

[53] W. Zheng, J.M. Nilles, D. Radisic, K.H. Bowen, J. Chem. Phys. 122 (2005) 071101.

[54] H. Kudo, C.H. Wu, H.R. Ihle, J. Nucl. Mat. 78 (1978) 380-389.

[55] H. Kudo, Nature 355 (1992) 432-434.

[56] P.v.R. Schleyer, E.U. Würthwein, E. Kaufmann, T. Clark, J. Am. Chem. Soc. 105 (1983) 5930-5932.

[57] C.H. Wu, Chem. Phys. Lett. 139 (1987) 357-359.

[58] H. Kudo and C.H. Wu, J. Nucl. Mat. 201 (1993) 261-266.

[59] P. Lievens, P. Thoen, S. Bouckaert, W. Bouwen, F. Vanhoutte, H. Weidele, and R. Silverans, Chem. Phys. Lett. 302 (1999) 571-576.

[60] E.U. Würthwein, P.v.R. Schleyer, and J.A. Pople, J. Am. Chem. Soc. 106 (1984) 6973-6978.

[61] A.I. Boldyrev and P.v.R. Schleyer, J. Am. Chem. Soc. 113 (1991) 9045-9054.

[62] H. Kudo, K.F. Zmbov, Chem. Phys. Lett. 187 (1991) 77-80.

[63] O. Hampe, G.M. Koretsky, M. Gegenheimer, C. Huber, M.M. Kappes, J. Gauss, J. Chem. Phys. 107 (1997) 7085-7095.

[64] S. Neukermans, E. Janssens, H. Tanaka, R.E. Silverans, P. Lievens, K. Yokoyama, H. Kudo, J. Chem. Phys. 119 (2003) 7206-7213.

[65] B.C. Guo, K.P. Kerns, A.W. Castleman, Jr., Science 255 (1991) 1411.

[66] P. Lievens, P. Thoen, S. Bouckaert, W. Bouwen, F. Vanhoutte, H. Weidele, R. Silverans, A. Navarro-Vázquez, and P. Schleyer, J. Chem. Phys. 110 (1999) 10316-10329.

[67] P. Lievens, P. Thoen, S. Bouckaert, W. Bouwen, F. Vanhoutte, H. Weidele, R. Silverans, A. Navarro-Vázquez, and P. Schleyer, Eur. Phys. J. D 9 (1999) 289-295.

[68] T. Bergmann, H. Limberger, T.P. Martin, Phys. Rev. Lett. 60 (1988) 1767-1770

[69] H. Limberger and T. Martin, J. Chem. Phys. 90 (1989) 2979-2991.

[70] T. Bergmann, T.P. martin, J. Chem. Phys. 90 (1989) 2848-2855.

[71] R. Antoine, P. Dugourd, D. Rayane, E. Benichou, and M. Broyer, J. Chem. Phys. 107 (1997) 2664-2672.

[72] C. Brechignac, P. Cahuzac, M. de Frutos, and P. Garnier, Z. Phys. D 42 (1997) 303-307.

[73] V. Boutou, M. Lebault, A. Allouche, C. Bordas, F. Paulig, J. Viallon, and J. Chevaleyre, Phys. Rev. Lett. 80 (1998) 2817-2820.

[74] V. Boutou, M. Lebault, A. Allouche, C. Bordas, F. Paulig, J. Viallon, and J. Chevaleyre, J. Chem. Phys. 112 (2000) 6228-6236.

[75] P.J. Ziemann, A.W. Castleman, J. Chem. Phys. 94 (1991) 718-728.

[76] T.P. Martin, T. Bergmann, J. Chem. Phys. 90 (1989) 6664-6667.

[77] F.L. King, B.I. Dunlap, D.C. Parent, J. Chem. Phys. 94 (1991) 2578-2587.

[78] X. Li, L.S. Wang, Phys. Rev. B 65 (2002) 153404.

[79] H. Kawamata, Y. Negishi, A. Nakajima, K. Kaya, Chem. Phys. Lett. 337 (2001) 255-262.

[80] B.D. Leskiw, A.W. Castleman, Chem. Phys. Lett. 316 (2000) 31-36.

[81] E. Janssens, S. Neukermans, F. Vanhoutte, R.E. Silverans, P. Lievens, A. Navarro-Vázquez, P.v.R. Schleyer, J. Chem. Phys. 118 (2003) 5862-5871.

[82] O.P. Charkin, D.O. Charkin, N.M. Klimenko, A.M. Mebel, Chem. Phys. Lett. 365 (2002) 494-504.

[83] D.E. Bergeron, A.W. Castleman Jr., T. Morisato, S.N. Khanna, Science 304 (2004) 84-87.

[84] D.E. Bergeron, P.J. roach, A.W. Castleman Jr., N.O. Jones, S.N. Khanna, Science 307 (2005) 231-235.

[85] S. Neukermans, E. Janssens, H. Tanaka, R.E. Silverans, P. Lievens, Phys. Rev. Lett. 90 (2003) 033401.

[86] E. Janssens, H. Tanaka, S. Neukermans, R.E. Silverans, P. Lievens, New. J. Phys. 5 (2003) 46.1-10.

[87] E. Janssens, H. Tanaka, S. Neukermans, R.E. Silverans, P. Lievens, Phys. Rev. B 69 (2004) 085402.

[88] H. Tanaka, S. Neukermans, E. Janssens, R.E. Silverans, P. Lievens, J. Am. Chem. Soc. 125 (2003) 2862-2863.

[89] S. Dennler, J.L. Ricardo-Chavez, J. Morillo, G.M. Pastor, Eur. Phys. J. D 24, 2003, 237-240.

[90] W.J.C. Menezes, M.B. Knickelbein, Z. Phys. D 26 (1993) 322-324.

[91] H. Tanaka, S. Neukermans, E. Janssens, R.E. Silverans, and P. Lievens, J. Chem. Phys. 119 (2003) 7115-7123.

[92] M.B. Torres, E.M. Fernandez, and L.C. Balbas, Phys. Rev. B 71 (2005) 155412.

[93] X. Li, B. Kiran, L.F. Cui, L.S. Wang, Phys. Rev. Lett. 95 (2005) 253401.

[94] F. Furche, R. Ahlrichs, P. Weis, C. Jacob, S. Gilb, T. Bierweiler, M.M. Kappes, J. Chem. Phys. 117 (2002) 6892-6990.

[95]H. Häkkinen, B. Yoon, U. Landman, X. Li, H.J. Zhai, L.S. Wang, J. Phys. Chem. A 107 (2003) 6168-6175.

[96] P. Pyykkö, Angew. Chem. Int. Ed. 43 (2004) 4412-4456.

[97] C.W. Corti, Gold Bulletin 37 (2004) 12-19.

[98] P. Pyykkö, N. Runeberg, Ang. Chem. Int. ed. 41 (2002) 2174-2176.

[99] X. Li, B. Kiran, J. Li, H.J. Zhai, L.S. Wang, Ang. Chem. Int. Ed. 41 (2002)4786-4789.

[100] J. Autschbach, B.A. Hess, M.P. Johansson, J. Neugebauer, M. Patzschke, P. Pyykkö, M. Reiher, D. Sundholm, Phys. Chem. Chem. Phys. 6 (2004) 11-22.

[101] K. Manninen, P. Pyykkö, and H. Hakkinnen, Phys. Chem. Chem. Phys. 7 (2005) 2208-2211.

[102] M. Laupp, J. Strähle, Angew. Chem. Int. Ed. 33 (1994) 207-209.

[103] R. Arratia-Pérez, L. Hernández-Acevedo, Chem. Phys. Lett. 303 (1999) 641-648.

[104] Q. Sun, Q. Wang, Y. Kawazoe, P. Jena, Eur. Phys. J. D 29 (2004) 231-234.

[105] W. Fa, J. Dong, J. Chem. Phys. 124 (2006) 114310.

[106] M.P. Johansson, D. Sundholm, J. Vaara, Angew. Chem. Int. Ed. 43 (2004) 2678-2681.

[107] Y. Gao, X.C. Zeng, J. Am. Chem. Soc. 127 (2005) 3698-3699.

[108] J. Wang, J. Jellinek, J. Zhao, Z. Chen, R.B. King, P.v.R. Schleyer, J. Phys. Chem. A 109 (2005) 9265-9269.

[109] S. Bulusu, X. Li, L.S. Wang, X.C. Zeng, Proc. Nat. Acad. Sci. 103 (2006) 8326-8330.

[110] J. Li, X. Li, H.J. Zhai, L.S. Wang, Science 299 (2003) 864-867.

[111] Y. Gao, S. Bulusu, X.C. Zeng, J. Am. Chem. Soc. 127 (2005) 15680-15681.

[112] Y. Gao, S. Bulusu, X.C. Zeng, unpublished.

[113] M. Walter, H. Häkkinen, Phys. Chem. Chem. Phys. (2006) in press.

[114] F. Naumkin, Phys. Chem. Chem. Phys. 8 (2006) 2539-2545.

[115] E. Janssens, S. Neukermans, H.M.T. Nguyen, M.T. Nguyen, P. Lievens, Phys. Rev. Lett. 94 (2005) 113401.

[116] E. Janssens, S. Neukermans, X. Wang, N. Veldeman, R.E. Silverans, P. Lievens, Eur. Phys. J. D, 34 (2005) 23-27.

[117] E. Janssens, X.J. Hou, M.T. Nguyen, P. Lievens, J. Chem. Phys. 124 (2006) 184319.

[118] E. Janssens, T. Van Hoof, N. Veldeman, S. Neukermans, M. Hou, P. Lievens, Int. J. Mass. Spectrom. 252 (2006) 38-46.

[119] X.J. Hou, E. Janssens, P. Lievens, M.T. Nguyen, Chem. Phys. (2006) in press.

[120] Q. Sun, X.G. Gong, Q.Q. Zheng, D.Y. Sun, G.H. Wang, Phys. Rev. B 54 (1996) 10896-10904.

[121] Q. Sun, Q. Wang, J.Z. Yu, Z.Q. Li, J.T. Wang, Y. Kawazoe, J. Phys. I 7 (1997) 1233-1244.

[122] S.Y. Wang, J.Z. Yu, H. Mizuseki, Q. Sun, C.Y. Wang, Y. Kawazoe, Phys. Rev. B 70 (2004) 165413.

[123] K. Jackson, B. Nellermoe, Chem. Phys. Lett. 254 (1996) 249-256.

[124] K. Jackson, E. Kaxiras, and M.R. Pederson, J. Phys. Chem. 98 (1994) 7805-7810.

[125] S.M. Beck, J. Chem. Phys. 87 (1987) 4233-4234.

[126] R.B. King, Z. Phys. D 18 (1991) 189-191.

[127] V. Kumar and Y. Kawazoe, Phys. Rev. B 65 (2002) 073404.

[128] H. Hiura, T. Miyazaki, T. Kanayama, Phys. Rev. Lett. 86 (2001) 1733-1736.

[129] S.N. Khanna, B.K. Rao, P. Jena, S.K. Nayak, Chem. Phys. Lett. 373 (2003) 433-438.

[130] S.N. Khanna, B.K. Rao, P. Jena, Phys. Rev. Lett. 89 (2002) 016803.

[131] R.H. Crabtree, The organometallic chemistry of the transition metals, 3rd ed. (2001) New York Wiley

[132] K. Koyasu, M. Akutsu, M. Mitsui, A. Nakajima, J. Am. Chem. Soc. 127 (2005) 4998-4999.

[133] K. Jackson and B. Nellermoe, Chem. Phys. Lett. 254 (1996) 249-256.

[134] F. Hagelberg, I. Yanov, J. Leszczynski, J. Mol. Struc. 487 (1999) 183-192.

[135] V. Kumar and Y. Kawazoe, Phys. Rev. Lett. 87 (2001) 045503.

[136] C Xiao, F. Hagelberg, W.A. Lester, Phys. Rev. B 66 (2002) 075425.

[137] F. Hagelberg, C. Xiao, W.A. Lester, Phys. Rev. B 67 (2003) 035426.

[138] P. Sen and L. Mitas, Phys. Rev. B 68 (2003) 155404.

[139] T. Miyazaki, H. Hiura, T. Kanayama, Phys. Rev. B 66 (2002) 121403.

[140] V. Kumar, C. Majumder, Y. Kawazoe, Chem. Phys. Lett. 363 (2002) 319-322.

[141] S.N. Khanna, B.K. Rao, P. Jena, Phys. Rev. Lett. 89 (2002) 016803.

[142] J. Lu and S. Nagase, Phys. Rev. Lett. 90 (2003) 115506.

[143] V. Kumar, T.M. Briere, Y. Kawazoe, Phys. Rev. B 68 (2003) 155412.

[144] V. Kumar, Comp. Mat. Science 30 (2004) 260-268.

[145] C. Majumder and S.K. Kulshreshtha, Phys. Rev. B (2004) 245426.

[146] H. Kawamura, V. Kumar, Y. Kawazoe, Phys. Rev. B 70 (2004) 245433.

[147] H. Kawamura, V. Kumar, Y. Kawazoe, Phys. Rev. B 71 (2005) 075423.

[148] A.K. Singh, V. Kumar, Y. Kawazoe, Phys. Rev. B 71 (2005) 115429.

[149] V. Kumar and Y. Kawazoe, Appl. Phys. Lett. 80 (2002) 859-861.

[150] V. Kumar and Y. Kawazoe, Phys. Rev. Lett. 88 (2002) 235504.

[151] V. Kumar and Y. Kawazoe, Appl. Phys. Lett. 83 (2003) 2677-2679.

[152] V. Kumar, Eur. Phys. J. D 24 (2003) 227-232.

[153] V. Kumar, A.K. Singh, Y. Kawazoe, Nano Lett. 4 (2004) 677-681.

[154] V. Kumar, Comp. Mat. Science 36 (2006) 1-11.

[155] S.M. Beck, J. Chem. Phys. 90 (1989) 6306-6312.

[156] H. Hiura, T. Miyazaki, T. Kanayama, Phys. Rev. Lett. 86 (2001) 1733-1736.

[157] M. Ohara, K. Koyasu, A. Nakajima, K. Kaya, Chem. Phys. Lett. 371 (2003) 490-497.

[158] X. Zhang, Z. Tang, Z. Gao, Rap. Comm. Mass Spec. 17 (2003) 621-626.

[159] X. Zhang G. Li, X. Xing, X. Zhao, Z. Tang, Z. Gao, Rap. Comm. Mass. Spec. 15 (2001) 2399-2403.

[160] S. Neukermans, E. Janssens, Z.F. Chen, R.E. Silverans, P.v.R. Schleyer, and P. Lievens, Phys. Rev. Lett. 92 (2004) 163401.

[161] E.N. Esenturk, J. Fettinger, Y.F. Lam, B. Eichhorn, Ang. Chem. Int. Ed. 43 (2004) 2132-2134.

[162] Z. Chen, S. Neukermans, X. Wang, E. Janssens, Z. Zhou, R.E. Silverans, R.B. King, P.v.R. Schleyer, P. Lievens, J. Am. Chem. Soc. 128 (2006) 12829-12834.

[163] E.N. Esenturk, J. Fettinger, B. Eichhorn, J. Am. Chem. Soc. 128 (2006) 9178-9186.

[164] L.F. Cui, X. Huang, L.M. Wang, J. Li, L.S. Wang, J. Phys. Chem. A, 110 (2006) 10169-10172.

[165] L.F. Cui, X. Huang, L.M. Wang, D. Y. Zubarev, A.I. Boldyrev, J. Li, L.S. Wang, J. Am. Chem. Soc. 128 (2006) 8390-8391.

[166] D.L. Chen, W.Q. Tian, W.C. Lu, C.C. Sun, J. Chem. Phys. 124 (2006)154313.

[167] S. Neukermans, X. Wang, N. Veldeman, E. Janssens, R.E. Silverans, P. Lievens, Int. J. Mass. Spectrom. 252 (2006) 145-150.

[168] Z. Chen, C.S. Wannere, C. Corminboeuf, R. Puchta, P.v.R. Schleyer, Chem. Rev. 105 (2005) 3842-3888.